Novel Statistical Wideband MIMO V2V Channel Modeling Using Unitary Matrix Transformation Algorithm

Hao Jiang, *Member, IEEE*, Baiping Xiong, Zaichen Zhang, *Senior Member, IEEE*,
Jiangfan Zhang, *Member, IEEE*, Hongming Zhang, *Member, IEEE*, Jian Dang, *Senior Member, IEEE*,
and Liang Wu, *Member, IEEE*

Abstract— For efficiently investigating the statistical properties of wideband multiple-input multiple-output (MIMO) channels for vehicle-to-vehicle (V2V) communication scenarios, we propose a novel computationally efficient solution to estimate the parameters of the proposed channel model for different propagation delays in this paper. To be specific, we first introduce a Unitary transformation method to estimate the propagation delay of the proposed channel model for the first tap in the preliminary stage before the mobile transmitter (MT) and mobile receiver (MR) move. Then, we estimate the real-time angular parameters based on the estimated delay and moving time/directions/velocities of the MT and MR. Furthermore, we estimate the expressions of the real-time complex channel impulse responses (CIRs), which can be used to characterize the physical properties of the proposed channel model, by substituting the estimates of the time-varying AoD and AoA and model parameters into the complex CIRs. Numerical results of the channel characteristics fit the theory results very well, which validate that the proposed channel model is practical for characterizing the beyond fifth-generation (B5G) V2V communication systems.

Index Terms— Wideband MIMO V2V channel model, unitary transformation method, propagation delay, complex CIR.

I. INTRODUCTION

THE beyond fifth-generation (B5G) systems will enable people to access and share information in a wide range of all spectrums, global coverage, and full applications scenarios with extremely low latency and very high data rate [1]. In contrast to 5G channel models, B5G should combine different technologies and disciplines, such as high-mobility, multiple mobility, uncertainty of motion trajectory, non-stationarity in time/frequency/spatial domains, etc, which causes high complexity of modeling approach, model parameters and simulation time. Vehicle-to-vehicle (V2V) communications, which aims to minimize traffic accidents and foster the development of new applications, are expected to be hot research topics for B5G wireless communication systems [2]. In order to study access link and network performance in realistic V2V propagation conditions, and compare different B5G communication solutions, it is important to gain insight into the statistical properties between mobile transmitters (MTs) and mobile receivers (MRs) [3].

A. Related Work

To investigate the statistical properties of multiple-input multiple-output (MIMO) wireless channels, the existing literatures [4]- [10] adopted geometry-based stochastic models (GBSMs), which employ a geometric approach to represent the propagation environments between a transmitter and a receiver in multipath channels. To be specific, the authors in [4] and [5] proposed Ricean channel models to study the statistical propagation properties, which adopted an ellipse model to depict the distribution of scattering environments

Hao Jiang is with the College of Artificial Intelligence, Nanjing University of Information Science and Technology, Nanjing 210044, China, also with the National Mobile Communications Research Laboratory, Southeast University, Nanjing 210096, China, and also with the State Key Laboratory of Rail Traffic Control and Safety, Beijing Jiaotong University, Beijing 100044, China (e-mail: jianghao@nuist.edu.cn).

Baiping Xiong, Jian Dang, and Liang Wu are with the National Mobile Communications Research Laboratory, Southeast University, Nanjing 210096, China (e-mail: xiongbp@seu.edu.cn; dangjian@seu.edu.cn; wuliang@seu.edu.cn).

Zaichen Zhang is with the National Mobile Communications Research Laboratory, Southeast University, Nanjing 210096, China, and also with the Purple Mountain Laboratory, Nanjing 211111, China (e-mail: zczhang@seu.edu.cn).

Jiangfan Zhang is with the Department of Electrical and Computer Engineering, Missouri University of Science and Technology, Rolla, MO 65409 USA (e-mail: jiangfanzhang@mst.edu).

Hongming Zhang is with the School of Information and Communication Engineering, Beijing University of Posts and Telecommunications, Beijing 100876, China (e-mail: zhanghm@bupt.edu.cn).

Color versions of one or more figures in this article are available at https://doi.org/10.1109/TWC.2021.3063762.

Digital Object Identifier 10.1109/TWC.2021.3063762

in mobile radio communication scenarios. The authors in [6] proposed a statistical geometric propagation model for mobile-to-mobile (M2M) communication scenarios, which assumed that the propagation components emerged from the MT to the MR experience single interaction in wireless channels. Meanwhile, the distribution of scatterers are assumed to be uniformly distributed within a two-ring model between a transmitter and a receiver. It has been proved in [7] that the propagation components with different delays have different contributions to the propagation characteristics; therefore, we should consider the statistical properties of wideband channels for different delays, i.e., per-tap channel statistics. In light of this, the authors in [8] adopted multiple confocal ellipse models to describe the distribution of scatterers for different propagation delays; therefore, the statistical propagation properties of V2V channels for different taps can be derived and investigated. The authors in [9] and [10] introduced multiple confocal semi-ellipsoid models and multiple confocal elliptic-cylinder models, respectively, to investigate the statistical properties of wideband V2V channels for different delays.

For the efficient evaluation of the performance of wireless communication systems, a variety of angular estimation algorithms have been proposed in the existing studies. To be specific, the authors in [11] proposed Rayleigh fading channel models in space-, time-, and frequency-domains, whose results demonstrated that the models are able to effectively characterize the performance of discrete-time MIMO communication systems. Xiao *et al.* [12] proposed an estimation algorithm in a Clarke channel model, the results demonstrated that the algorithm could be used to reduce the variation of temporal correlations of a fading realization. It is worth mentioning that the direction of arrivals (DoAs) estimation of multiple narrowband signals is a fundamental problem that arises in various engineering applications. In light of this, various algorithms have been studied by providing low computational complexity of DoA estimators for many practical communication systems. It has been stated in [13] that the Unitary transformation is one of the most representative solutions for reducing the complexity, which achieves high computational efficiency via real-domain computations. In [14], the authors transformed a Hermitian persymmetric covariance matrix into a real symmetric matrix using a unitary transformation, which depends on the number of sensors. Furthermore, the authors in [15] proposed an estimated wideband GBSM for V2V communication environments, which is based on an angle-of-departure (AoD) and angle-of-arrival (AoA) estimation algorithm, to determine the ellipse scattering region and to efficiently study the V2V channel characteristics for different propagation delays, i.e., per-tap channel statistics. In [16], the authors proposed a unitary transformation method in element space by exploiting the centro-symmetry of the uniform circular array (UCA), which transformed the DoA estimation algorithms into real-domain computations; therefore greatly decrease the computational complexity and the hardware implementation complexity. However, in [16], the impact of the physical properties of wireless channels on the performance of angular estimation algorithms was not considered.

B. Motivations

It is worth mentioning that when the MT and MR are in motion, due to the high computational complexity and the non-real-time property of the estimating algorithm, it is infeasible to acquire the real-time complex channel impulse responses (CIRs) to characterize the wireless communications by using the existing methods. To address this issue, we need to propose a computationally efficient solution to estimate the real-time angular parameters for different time, by utilizing the estimated angular parameters in the preliminary stage and the kinetics (e.g., moving velocities/directions) of the MT and MR in the real-time stage. This motivates us to propose a computationally efficient solution with low complexity to investigate the MIMO V2V channel characteristics.

C. Main Contributions

In this paper, we propose a statistical wideband MIMO V2V channel model based on a Unitary matrix transformation algorithm. The main contributions are summarized as follows:

- The complex CIRs, which can be used to characterize the physical properties of wireless channels, are transformed into real-domain based on a Unitary transform algorithm with the goal of reducing the computational complexity of the channel modeling.
- We employ a Unitary transformation algorithm to estimate the MIMO channel models for V2V communication scenarios, where the propagation paths induced by the clusters with different delays are located at different taps. Numerical channel characteristics of the proposed channel model are very close to the theoretical results, which validate that the algorithm can provide accurate estimates of the channel parameters, and hence, can further improve the computational efficiency of the proposed channel model for real wireless communication environments.
- By adjusting the model parameters, the proposed MIMO V2V wideband non-stationary channel model is able to describe a variety of wireless communication scenarios. Specifically, the model can be used to describe the wide-sense stationary uncorrelated scattering (WSSUS) channels as the MT and MR are static. In addition, when we only consider the complex CIRs for a specific tap, the model can be used to characterize narrowband channels, i.e., frequency-nonselective channels.

The remainder of this paper is organized as follows. Section II describes the system channel model for the proposed wideband MIMO V2V communication environments. In Section III, we introduce a Unitary algorithm to estimate the propagation delay of the proposed channel model for the first tap in a preliminary stage before the MT and MR move. Then, we estimate the angular parameters for other taps in the real-time stage. In Section IV, numerical results and discussions are provided. Finally, our conclusions are presented in Section V.

II. SYSTEM CHANNEL MODEL

In this section, we propose a novel wideband MIMO channel model for V2V communication systems with multiple
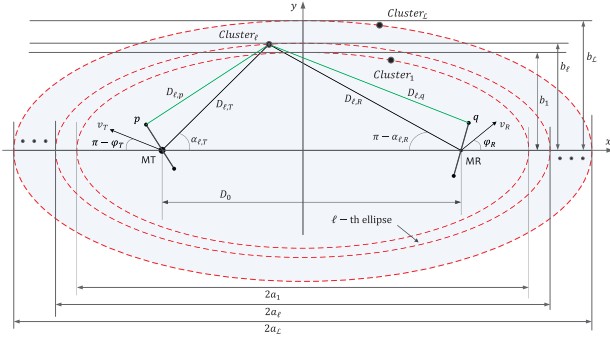
Fig. 1. Illustration of the proposed wideband MIMO V2V channel model.

Fig. 2. Mobile properties of the proposed MIMO V2V channel model.

clusters to describe different taps, where the MT and MR are equipped with the uniform linear arrays (ULAs) consisting of M_T and M_R omni-directional antennas [17], respectively, as shown in Fig. 1. Let us define the line connecting the center of the MT antenna array and that of the MR array as the x-axis, which remains unchanged even when the MT and MR are in motion. The existing literature adopted an ellipse model with a MT and a MR located at the foci to determine the waves with the same propagation delays, while different ellipses correspond to different propagation delays. In the proposed channel model, we assume that there are N_ℓ scatterers within the cluster lie on the ellipse model, where the semi-lengths on the major axis (i.e., x-axis) and minor axis (i.e., y-axis) of the ℓ-th ($\ell = 1, 2, \ldots, \mathcal{L}$) ellipse are denoted as a_ℓ and b_ℓ, respectively. It is assumed that the direct link between the MT and MR are blocked by interfering objects, and therefore the waves emitted from the MT experience multiple rays reflected by the clusters before reaching the MR. We assume that every ray induced by the same cluster approximately has the same propagation distance as that from the center of the corresponding antenna array. A similar assumption was made in [18]. Therefore, it is reasonable to use the same AoD and AoA to characterize the multi-paths propagation from the transmit/receive antennas to the same cluster. The AoD and AoA of the propagation components via the ℓ-th cluster are denoted as $\alpha_{\ell,T}$ and $\alpha_{\ell,R}$, respectively. The distances from the central points of the MT and MR antenna arrays to the ℓ-th cluster are denoted as $D_{\ell,T}$ and $D_{\ell,R}$, respectively. Furthermore, the distances from the p-th ($p = 1, 2, \ldots, M_T$) antenna of the MT array and the q-th ($q = 1, 2, \ldots, M_R$) antenna of the MR array to the ℓ-th cluster are denoted as $D_{\ell,p}$ and $D_{\ell,q}$, respectively.

The physical properties of the proposed wideband MIMO channel model can be described by a matrix $\mathbf{H}(t, \tau) = [h_{pq}(t, \tau)]_{M_R \times M_T}$ of size $M_R \times M_T$, where $h_{pq}(t, \tau)$ represents the complex CIR between the p-th transmit antenna and q-th receive antenna, which is modeled as the superposition of the $\mathcal{L}$ resolvable non-line-of-sight (NLoS) components, i.e., [19]

$$h_{pq}(t, \tau) = \sum_{\ell=1}^{\mathcal{L}} \chi_\ell h_{\ell,pq}(t) \delta(\tau - \tau_\ell), \quad (1)$$

where χ_ℓ denotes the attenuation factor of the ℓ-th tap. The τ_ℓ is the propagation delay of the NLoS rays from the central
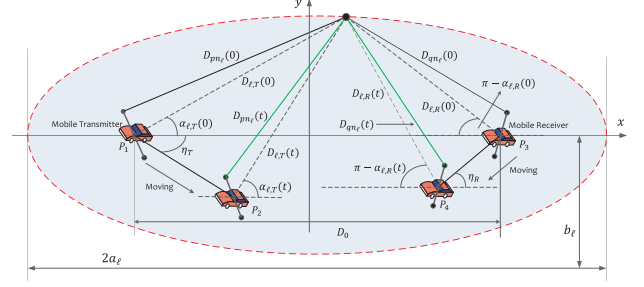
point of the MT antenna array to that of the MR antenna array. The complex channel response $h_{\ell,pq}(t)$ for NLoS rays, which is a random process, can be expressed as [20]

$$h_{\ell,pq}(t) = e^{j\left(\varphi_0 - 2\pi f_c \tau_{\ell,pq}\right)}$$
$$\times e^{j\frac{2\pi}{\lambda} v_T t \cos\left(\alpha_{\ell,T} - \eta_T\right)} e^{j\frac{2\pi}{\lambda} v_R t \cos\left(\alpha_{\ell,R} - \eta_R\right)}, \quad (2)$$

where f_c is the carrier frequency and λ is the carrier wavelength. The $\tau_{\ell,pq}$ is the propagation delay of the waves from the p-th transmit antenna to the q-th receive antenna via the NLoS components. Furthermore, v_T and v_R denote the moving velocities of the MT and MR, respectively; η_T and η_R are the moving directions of the MT and MR with respect to the positive direction of the x-axis in the channel model, respectively. Here, we should mention that the parameters v_T, v_R, η_T, and η_R are all set to be constant in this paper. Moreover, $\alpha_{\ell,T}$ and $\alpha_{\ell,R}$ are the AoD and AoA of the NLoS components, respectively. Finally, φ_0 is a random phase angle, which follows a uniform distribution in the interval from $-\pi$ to π, i.e., $\varphi_0 \sim [-\pi, \pi)$.

III. UNITARY BASED PROPAGATION DELAY ESTIMATION

As shown in Fig. 2, when the MT moves from the position P_1 to the position P_2, and the MR moves from the position P_3 to the position P_4, the time-varying AoD and AoA should be estimated to characterize the non-stationary properties of the proposed wideband MIMO V2V channel model in time domain [6]. To achieve this goal, we assume that the MR is able to receive the signal transmitted from the MT in the preliminary stage of the system, which is in correspondence with the time period before the motion of the MT and MR. Then, we propose a four-step computational solution to investigate the characteristics of the proposed channel model for different propagation delays at different moving time, which can be shown as follows:

First, we introduce a Unitary matrix algorithm to transform the complex CIR for the first tap in the preliminary stage into real-value domain. This aims at improving the computational efficiency of the algorithm to estimate the proposed channel model for the first tap. Therefore, the lengths of the semi-major and semi-minor axes of the ellipse channel model for the first tap, can be determined based on the estimated propagation delay of the proposed channel model for the first tap and the distance between the centers of the MT and MR antenna arrays;

Next, we estimate the lengths of the semi-major and semi-minor axes of the ellipse channel model for other taps based on the estimated ellipse model parameters for the first tap and the predefined delay resolution between the taps;

Moreover, for each time instant when the MT and MR are in motion, we estimate the real-time AoD and AoA based on the estimated model parameters for the first tap and the moving time/directions/velocities of the MT and MR;

Finally, by substituting the estimates of the time-varying AoD and AoA into the complex CIR in (1), we are able to estimate the complex CIR of the proposed channel model for other taps.

A. Estimation of the Propagation Delay for the First Tap

In the proposed channel model, the signals transmitted by the MT experience different propagation delays before reaching the MR. Assume that the MT and MR are in static during the initialization, i.e., $t = 0$. At this time, the propagation delay of the NLoS components is denoted as $\tau_{1,pq}(0)$. Hence the complex CIR can be expressed as [15]

$$h_{pq}(0, \tau) = \chi_1 e^{j\left(\varphi_0 - 2\pi f_c \tau_{1,pq}(0)\right)} \delta\left(\tau - \tau_1(0)\right), \qquad (3)$$

where $\tau_1(0) = \left(D_{1,T}(0) + D_{1,R}(0)\right)/c$ is the propagation delay of the waves from the central point of the MT antenna array to that of the MR array via the reflection of the cluster for the first tap, with $D_{1,T}(0)$ and $D_{1,R}(0)$ being the distances from the centers of the MT and MR antenna arrays to the cluster for the first tap, respectively. The $c = 3.0 \times 10^8$ m/s is the speed of light. We have that

$$D_{1,T}(0) = \frac{c^2 \tau_1^2(0) - D_0^2}{2c\tau_1(0) - 2D_0 \cos \alpha_{1,T}(0)}, \qquad (4)$$

$$D_{1,R}(0) = \frac{c^2 \tau_1^2(0) - D_0^2}{2c\tau_1(0) - 2D_0 \cos \alpha_{1,R}(0)}, \qquad (5)$$

where D_0 denotes the distance between the center points of the MT and MR antenna arrays. The $\alpha_{1,T}(0)$ is the AoD of the NLoS propagation components from the MT to the cluster for the first tap, $\alpha_{1,R}(0)$ is the AoA of the NLoS components from the MR to the cluster for the first tap. Furthermore, $\tau_{1,pq}(0) = \left(D_{1,p}(0) + D_{1,q}(0)\right)/c$ is the propagation delay from the p-th transmit antenna to the q-th receive antenna via the reflection of the cluster for the first tap, where $D_{1,p}(0)$ and $D_{1,q}(0)$ are the distances from the p-th transmit antenna and q-th receive antenna to the cluster, respectively, and they can be expressed as (6) and (7), as shown at the bottom of the page, respectively, as shown at the bottom of this page, where $k_p = (M_T - 2p + 1)/2$ and $k_q = (M_R - 2q + 1)/2$ with δ_T and δ_R denote the adjacent spacings between two different antenna

elements of the transmit and receive arrays, respectively. The ψ_T and ψ_R are the orientations of the transmit and receive antenna arrays relative to the positive direction of the x-axis, respectively.

Subsequently, the received noisy signal of the q-th receive antenna for the first tap can be expressed as

$$
\begin{aligned}
y_q(\tau) &= \sum_{p=1}^{M_T} h_{pq}(0, \tau) * s_p(\tau) \\
&= \sum_{p=1}^{M_T} \chi_1 e^{j\left(\varphi_0 - 2\pi f_c \tau_{1,pq}(0)\right)} s_p\left(\tau - \tau_1(0)\right) + n_q(\tau),
\end{aligned}
$$
$$(8)$$

where $s_p(\tau)$ denotes the signal transmitted by the p-th transmit antenna, $n_q(\tau)$ is the received complex noise of the q-th receive antenna, and $*$ is the convolution operator. According to the Nyquist sampling theorem [21], the received continuous time noisy signal $y_q(\tau)$ can be represented by the discrete sampling sequences $\{y_q(1T_0), \ldots, y_q(kT_0), \ldots, y_q(KT_0)\}$ without lossing any information. The K time instances sampling version of the q-th received signal, denoted by $\mathbf{y}_q \in \mathbb{C}^K$, can be written as [22]

$$
\begin{aligned}
\mathbf{y}_q &= \left[y_q(1T_0), y_q(2T_0), \ldots, y_q(kT_0), \ldots, y_q(KT_0) \right] \\
&= \mathbf{m}_q + \mathbf{n}_q,
\end{aligned}
$$
$$(9)$$

where

$$\mathbf{m}_q = \sum_{p=1}^{M_T} \chi_1 \ e^{j\left(\varphi_0 - 2\pi f_c \tau_{1,pq}(0)\right)} \begin{bmatrix} s_p(1T_0 - \tau_1(0)) \\ \vdots \\ s_p(kT_0 - \tau_1(0)) \\ \vdots \\ s_p(KT_0 - \tau_1(0)) \end{bmatrix}^T, \qquad (10)$$

$$\mathbf{n}_q = \begin{bmatrix} n_q(1T_0) \\ \vdots \\ n_q(kT_0) \\ \vdots \\ n_q(KT_0) \end{bmatrix}^T, \qquad (11)$$

where the superscript $[\cdot]^T$ denotes the transpose operator, $s_p(kT_0 - \tau_1(0))$ is the k-th $(k = 1, 2, \ldots, K)$ sample of the signal transmitted by the p-th transmit antenna via the NLoS components. Furthermore, $n_q(kT_0)$ is the k-th temporal sample of the received noise $n_q(\tau)$, and $T_0 = 1/f_s$ is the sampling period.

Therefore, the vectorized received signal at the MR with K samples, denoted by $\mathbf{y} \in \mathbb{C}^{M_R K \times 1}$, can be

$$D_{1,p}(0) = \sqrt{D_{1,T}^2(0) + (k_p \delta_T)^2 - 2D_{1,T}(0)k_p \delta_T \cos\left(\alpha_{1,T}(0) - \psi_T\right)}, \qquad (6)$$

$$D_{1,q}(0) = \sqrt{D_{1,R}^2(0) + (k_q \delta_R)^2 - 2D_{1,R}(0)k_q \delta_R \cos\left(\alpha_{1,R}(0) - \psi_R\right)} \qquad (7)$$

expressed as

$$
\begin{aligned}
\mathbf{y} &= [\mathbf{y}_1, \mathbf{y}_2, \ldots, \mathbf{y}_q, \ldots, \mathbf{y}_{M_R}]^T \\
&= \underbrace{[\mathbf{m}_1, \mathbf{m}_2, \ldots, \mathbf{m}_q, \ldots, \mathbf{m}_{M_R}]^T}_{\mathbf{m}} \\
&\quad + \underbrace{[\mathbf{n}_1, \mathbf{n}_2, \ldots, \mathbf{n}_q, \ldots, \mathbf{n}_{M_R}]^T}_{\mathbf{n}}.
\end{aligned}
\tag{12}
$$

Assume that the elements in the noise vector $\mathbf{n} \in \mathbb{C}^{M_R K}$ are independent and identically distributed (i.i.d) to each other [23], i.e., $\mathbf{n} \sim \mathcal{CN}(\mathbf{0}, \sigma^2 \mathbf{I}_{M_R K})$, where $\mathbf{I}_{M_R K}$ denotes a $M_R K$ dimensional vector with all elements equal to one, e.g., $\mathbf{I}_{M_R K} = [1, 1, \ldots, 1]^T$, and σ^2 is the noise power. It is worth mentioning that the existing literature mainly adopts the complex CIRs to characterize the statistical properties of wireless channels, which in principle brings us high computational complexity. To address this issue, we propose a Unitary matrix algorithm to transform the complex CIR in the preliminary stage into the real-value domain, which aims at improving the computational efficiency of the estimation algorithm to estimate the propagation delay of the proposed channel model for the first tap. Then, the complex CIR in the real-time stage can be estimated based on the aforementioned estimated propagation delay and moving time/directions/velocities of the MT and MR. The detailed derivations of the Unitary transformation algorithm will be discussed below.

B. Unitary Transformation Method

Here, we introduce the basic properties of centro-Hermitian matrices [24].

Definition 1: For an arbitrary $\xi \times \gamma$ dimensional complex matrix $\mathbf{X}$, the matrix is centro-Hermitian if it satisfies

$$
\boldsymbol{\Pi}_\xi \mathbf{X}^* \boldsymbol{\Pi}_\gamma = \mathbf{X},
\tag{13}
$$

where the superscript * denotes the complex conjugate operation. The matrices $\boldsymbol{\Pi}_\xi$ and $\boldsymbol{\Pi}_\gamma$ are the $\xi \times \xi$ and $\gamma \times \gamma$ dimensional symmetric permutation matrices, respectively, with ones on their antidiagonal and zeros elsewhere, i.e., [25]

$$
\boldsymbol{\Pi}_{\xi(\gamma)} =
\begin{bmatrix}
 & & 1 \\
 & \cdot^{\cdot^{\cdot}} & \\
1 & &
\end{bmatrix}
\in \mathbb{R}^{\xi(\gamma) \times \xi(\gamma)}.
\tag{14}
$$

It should be noted that here we have $\boldsymbol{\Pi}_{\xi(\gamma)}^2 = \mathbf{I}_{\xi(\gamma)}$, where $\mathbf{I}_{\xi(\gamma)}$ denotes the $\xi(\gamma) \times \xi(\gamma)$ dimensional identity matrix. It deserves to mention that an arbitrary real matrix $\mathbf{R}$ is a special form of the complex matrix, with its imaginary parts equal to zero, i.e., $\mathrm{Im}\{\mathbf{R}\} = \mathbf{0}$; therefore, the *Definition 1* also applies to real matrices [26].

Definition 2: For an arbitrary $\xi \times \gamma$ dimensional complex matrix $\mathbf{Q}$, if it satisfies

$$
\boldsymbol{\Pi}_\xi \mathbf{Q}^* = \mathbf{Q},
$$

then the matrix $\mathbf{Q} \in \mathbb{C}^{\xi \times \gamma}$ is called left $\boldsymbol{\Pi}$-real.

For a real matrix $\mathbf{R}$, the corresponding *left $\boldsymbol{\Pi}$-real* matrix can be obtained by premultiplying a *left $\boldsymbol{\Pi}$-real* matrix $\mathbf{Q}$, which means that the matrix $\mathbf{QR}$ is *left $\boldsymbol{\Pi}$-real*. Note that the expressions of *left $\boldsymbol{\Pi}$-real* matrices are different as the

dimensional number varies, which can be separated into the even and odd cases, respectively, and they are written as [27], [28]

$$
\mathbf{Q}_{2\xi} = \frac{1}{\sqrt{2}}
\begin{bmatrix}
\mathbf{I}_\xi & j\mathbf{I}_\xi \\
\boldsymbol{\Pi}_\xi & -j\boldsymbol{\Pi}_\xi
\end{bmatrix}
\in \mathbb{C}^{2\xi \times 2\xi},
\tag{15}
$$

$$
\mathbf{Q}_{2\xi+1} = \frac{1}{\sqrt{2}}
\begin{bmatrix}
\mathbf{I}_\xi & \mathbf{0}_\xi & j\mathbf{I}_\xi \\
\mathbf{0}_\xi^T & \sqrt{2} & \mathbf{0}_\xi^T \\
\boldsymbol{\Pi}_\xi & \mathbf{0}_\xi & -j\boldsymbol{\Pi}_\xi
\end{bmatrix}
\in \mathbb{C}^{(2\xi+1) \times (2\xi+1)},
\tag{16}
$$

where $\mathbf{0}_\xi$ represents the ξ-dimensional column vector with all elements equal to zero, i.e., $\mathbf{0}_\xi = [0, \ldots, 0]^T$. In the following, we present the *Lee*'s main approach in [24] to establish an automorphism between centro-Hermitian matrices and real matrices.

Theorem 1: Let $\mathbf{Q}_\xi$ and $\mathbf{Q}_\gamma$ denote the arbitrary nonsingular left $\boldsymbol{\Pi}$-real matrices of size $\xi \times \xi$ and $\gamma \times \gamma$, respectively. Then the mapping relationship

$$
\mathbf{X} \rightarrow \mathbf{Q}_\xi^H \mathbf{X} \mathbf{Q}_\gamma
\tag{17}
$$

maps the arbitrary $\xi \times \gamma$ dimensional complex centro-Hermitian matrix $\mathbf{X}$ into a real matrix of the same size, i.e., $\mathbf{Q}_\xi^H \mathbf{X} \mathbf{Q}_\gamma \in \mathbb{R}^{\xi \times \gamma}$.

The vectorized $M_R K \times 1$ dimensional discrete sampling received signal vector $\mathbf{y}$ is not centro-Hermitian, therefore the mapping relationship in (17) cannot be directly applied to the complex received sampling signal vector $\mathbf{y}$ in (12). Here, we introduce the strategy of forward-backward averaging, which can be expressed as [29]

$$
\mathbf{Y}_{Pre} = \begin{bmatrix} \mathbf{y} & \boldsymbol{\Pi}_{M_R K} \mathbf{y}^* \end{bmatrix},
\tag{18}
$$

where $\mathbf{Y}_{Pre}$ denotes the $M_R K \times 2$ dimensional preprocessed matrix after forward-backward averaging. Note that the size of $\mathbf{y}$ is $M_R K \times 1$, and hence the measurements are doubled from K to $2K$ after forward-backward averaging, which results in an increased estimation accuracy [21]. Next, by postmultiplying a unitary permutation matrix, the centro-Hermitian form of the vectorized discrete sampling received signal can be expressed as

$$
\begin{aligned}
\mathbf{Y}_{CH} &= \mathbf{Y}_{Pre}
\begin{bmatrix}
\mathbf{I}_1 & \\
& \boldsymbol{\Pi}_1
\end{bmatrix} \\
&= \begin{bmatrix} \mathbf{y} & \boldsymbol{\Pi}_{M_R K} \mathbf{y}^* \boldsymbol{\Pi}_1 \end{bmatrix}.
\end{aligned}
\tag{19}
$$

Based on the *Theorem 1*, we transform the vectorized complex received sampling signal vector $\mathbf{y}$ into a real matrix, i.e.,

$$
\begin{aligned}
\mathbf{Y}_{Re} &= \mathbf{Q}_{M_R K}^H \mathbf{Y}_{CH} \mathbf{Q}_2 \\
&= \mathbf{Q}_{M_R K}^H \begin{bmatrix} \mathbf{y} & \boldsymbol{\Pi}_{M_R K} \mathbf{y}^* \boldsymbol{\Pi}_1 \end{bmatrix} \mathbf{Q}_2,
\end{aligned}
\tag{20}
$$

where $(\cdot)^H$ denote the conjugate operation, $\mathbf{Q}_{M_R K}$ and $\mathbf{Q}_2$ are the *left $\boldsymbol{\Pi}$-real* matrices of the even and odd order unitary matrices, respectively. They are derived according to the (15) and (16), respectively. The $\mathbf{Y}_{Re}$ is the corresponding $M_R K \times 2$ dimensional real matrix, i.e., $\mathbf{Y}_{Re} \in \mathbb{R}^{M_R K \times 2}$. Notice that when the number of the receive antenna elements is even or odd, the expressions of the real matrix $\mathbf{Y}_{Re}$ are different, which will be discussed in Appendix I.

Since the elements in the vector $\mathbf{y}_{Re}$ in (55) are assumed to be i.i.d, we can present the probability density function (PDF) of the multivariate normal distributed real vector $\mathbf{y}_{Re}$ as

$$f_{\mathbf{y}_{Re}}(\mathbf{y}_{Re}) = \frac{1}{\sqrt{(2\pi)^{4\Lambda K}|\boldsymbol{\Sigma}|}}$$
$$\times \exp\left\{-\frac{1}{2}(\mathbf{y}_{Re}-\boldsymbol{\mu})^T\boldsymbol{\Sigma}^{-1}(\mathbf{y}_{Re}-\boldsymbol{\mu})\right\}, \quad (21)$$

where $|\boldsymbol{\Sigma}| = \det(\boldsymbol{\Sigma})$ denotes the determinant of the covariance matrix $\boldsymbol{\Sigma}$, and $\boldsymbol{\mu}$ is the expectation of $\mathbf{y}_{Re}$, i.e., $\boldsymbol{\mu} = \mathbb{E}[\mathbf{y}_{Re}]$. Assume that the elements in the complex white Gaussian noise vector $\mathbf{n}$ are i.i.d, hence the $4\Lambda K \times 4\Lambda K$ dimensional covariance matrix $\boldsymbol{\Sigma}$ of the multivariate normal distributed real vector $\mathbf{y}_{Re}$ can be derived as $\boldsymbol{\Sigma} = \sigma^2 \mathbf{I}_{4\Lambda K}$. Therefore, the PDF in (21) can be further expressed as (22), as shown at the bottom of the page [30].

Finally, the propagation delay of the proposed channel model for the first tap can be estimated by solving the maximum likelihood estimation (MLE) problem as [31]

$$\hat{\tau}_1(0) = \arg\max_{\tau_1(0)} \ln\left(f_{\mathbf{y}_{Re}}(\mathbf{y}_{Re})\right), \quad (23)$$

where $\ln\left(f_{\mathbf{y}_{Re}}(\mathbf{y}_{Re})\right)$ denotes the likelihood function of the PDF in (23), and $\ln(\cdot)$ is the natural logarithm function. It is worth mentioning that the propagation delay $\hat{\tau}_1(0)$ can be estimated by using Newton-Raphson method. Therefore, the distances from the centers of the MT and MR antenna arrays to the cluster for the first tap in the preliminary stage can be respectively estimated as

$$\hat{D}_{1,T}(0) = \frac{c^2\hat{\tau}_1^2(0) - D_0^2}{2c\hat{\tau}_1(0) - 2D_0\cos\alpha_{1,T}(0)}, \quad (24)$$

$$\hat{D}_{1,R}(0) = \frac{c^2\hat{\tau}_1^2(0) - D_0^2}{2c\hat{\tau}_1(0) - 2D_0\cos\alpha_{1,R}(0)}, \quad (25)$$

It deserves to mention that the initial AoD $\alpha_{1,T}(0)$ and AoA $\alpha_{1,R}(0)$ for the first tap are both deterministic. The $\alpha_{1,R}(0)$ can be obtained by using the existing solutions, such as the eigenvalue decomposition-based methods [32], spectral searching-based method [33], deep learning-based method [34], and compressive sensing-based methods [35]. However, the $\alpha_{1,T}(0)$ can be estimated as

$$\hat{\alpha}_{1,T}(0) = \arctan\frac{\hat{D}_{1,R}(0)\sin\alpha_{1,R}(0)}{D_0 - \hat{D}_{1,R}(0)\cos\alpha_{1,R}(0)}. \quad (26)$$

The lengths of the semi-major and semi-minor axes of the ellipse model for the first tap can be respectively estimated as

$$\hat{a}_1 = \frac{1}{2}\left(\hat{D}_{1,T}(0) + \hat{D}_{1,R}(0)\right) = \frac{1}{2}c\hat{\tau}_1(0), \quad (27)$$

$$\hat{b}_1 = \sqrt{\hat{a}_1^2 - (D_0/2)^2}. \quad (28)$$

For other taps ($\ell > 1$), the lengths of the semi-major and semi-minor axes of the ellipse models can be respectively estimated as

$$\hat{a}_\ell = \hat{a}_1 + \frac{1}{2}(\ell - 1)c\tau', \quad (29)$$

$$\hat{b}_\ell = \sqrt{\hat{a}_\ell^2 - (D_0/2)^2}, \quad (30)$$

where τ' denotes the delay resolution between the taps. Therefore, the distances from the centers of the MT and MR antenna arrays to the ℓ-th cluster can be respectively estimated as

$$\hat{D}_{\ell,T}(0) = \frac{4\hat{a}_\ell^2 - D_0^2}{4\hat{a}_\ell - 2D_0\cos\alpha_{\ell,T}(0)}, \quad (31)$$

$$\hat{D}_{\ell,R}(0) = 2\hat{a}_\ell - \hat{D}_{\ell,T}(0), \quad (32)$$

where the AoD $\alpha_{\ell,T}(0)$ for other taps in the preliminary stage can be estimated as

$$\hat{\alpha}_{\ell,T}(0) = \arctan\frac{\hat{D}_{\ell,R}(0)\sin\alpha_{\ell,R}(0)}{D_0 - \hat{D}_{\ell,R}(0)\cos\alpha_{\ell,R}(0)}. \quad (33)$$

Similar as before, the initial $\alpha_{\ell,R}(0)$ for other taps can be obtained by using the existing methods. It is worth mentioning that the initial $\alpha_{\ell,T}(0)$ and $\alpha_{\ell,R}(0)$ for other taps are both deterministic.

Finally, it deserves to mention that the MT, MR, and clusters might be all in motion. For such scenario, we provide corresponding discussions in Appendix II.

C. Angular Parameters Estimations in the Real-Time Stage

In the real-time stage, the complex channel response between the p-th transmit antenna and q-th receive antenna can be expressed as (34), as shown at the bottom of the page, where $\alpha_{\ell,T}(t)$ and $\alpha_{\ell,R}(t)$ denote the time-varying AoD and AoA of the NLoS propagation components via the reflection of the ℓ-th cluster in the real-time stage, respectively, which can be estimated as

$$\hat{\alpha}_{\ell,T}(t) = \arctan\frac{\hat{D}_{\ell,T}(0)\sin\hat{\alpha}_{\ell,T}(0) - v_T t\sin\eta_T}{\hat{D}_{\ell,T}(0)\cos\hat{\alpha}_{\ell,T}(0) - v_T t\cos\eta_T}, \quad (35)$$

$$f_{\mathbf{y}_{Re}}(\mathbf{y}_{Re}) = \frac{1}{(2\pi\sigma^2)^{2\Lambda K}}\exp\left\{-\frac{1}{2\sigma^2}\sum_{\nu=1}^{4\Lambda K}\left[\left(\mathbf{y}_{Re}(\nu) - \boldsymbol{\mu}(\nu)\right)\left(\mathbf{y}_{Re}(\nu) - \boldsymbol{\mu}(\nu)\right)\right]\right\}$$
$$= \frac{1}{(2\pi\sigma^2)^{2\Lambda K}} \times \exp\left\{-\frac{1}{2\sigma^2}\sum_{\varepsilon=1}^{4}\sum_{\kappa=1}^{\Lambda}\sum_{k=1}^{K}\left[\mathbf{y}_{Re,\varepsilon,\kappa}^2(k) - 2\mathbf{y}_{Re,\varepsilon,\kappa}(k)\boldsymbol{\mu}_{\varepsilon,\kappa}(k) + \boldsymbol{\mu}_{\varepsilon,\kappa}^2(k)\right]\right\}. \quad (22)$$

$$h_{pq}(t,\tau) = \sum_{\ell=1}^{\mathcal{L}}\chi_\ell e^{j\left(\varphi_0 - 2\pi f_c\tau_{\ell,pq}(t)\right)} \times e^{j\frac{2\pi}{\lambda}v_T t\cos\left(\alpha_{\ell,T}(t) - \eta_T\right)}e^{j\frac{2\pi}{\lambda}v_R t\cos\left(\alpha_{\ell,R}(t) - \eta_R\right)}\delta\left(\tau - \tau_\ell(t)\right) \quad (34)$$

Algorithm 1 Procedure for the Proposed Channel Generation

Input:
Signal $\{x_p(\tau)\}_{p=1}^{M_T}$;
Generate the initial parameters, including the distance between the center of the transmit/receive antenna array and the cluster for the first tap;

Output:
The estimated channel matrix $\mathbf{H}(t, \tau) = [h_{pq}(t, \tau)]_{M_R \times M_T}$ in the real-time stage of the system.

1: Estimating the propagation delay $\hat{\tau}_1(0)$ based on the Unitary matrix transformation in the preliminary stage of the system.
2: Computing the lengths of the semi-major and semi-minor axes of the ellipse channel model for the first tap based on (27)-(28);
3: Computing the lengths of the semi-major and semi-minor axes for the ℓ-th tap by using the estimated model parameters for the first tap and predefined delay resolution between the taps based on (29)-(30);
4: Computing the time-varying distances $\hat{D}_{\ell,T}(t)$, $\hat{D}_{\ell,R}(t)$, $\hat{D}_{\ell,p}(t)$, and $\hat{D}_{\ell,q}(t)$ based on (37)-(40), respectively; as well as the time-varying AoD $\hat{\alpha}_{\ell,T}(t)$ and AoA $\hat{\alpha}_{\ell,R}(t)$ based on (35) and (36), respectively.
   Then, the time-varying statistical properties of the channel model can be described;
5: By substituting the complex fading envelope $h_{\ell,pq}(t)$ into (1), the complex CIR between the p-th transmit antenna and q-th receive antenna can be obtained. Then, the proposed channel model, which physical properties is characterized by the channel matrix $\mathbf{H}(t, \tau) = [h_{pq}(t, \tau)]_{M_R \times M_T}$, can be generated.

$$\hat{\alpha}_{\ell,R}(t) = \arctan \frac{\hat{D}_{\ell,R}(0) \sin \alpha_{\ell,R}(0) - v_R t \sin \eta_R}{\hat{D}_{\ell,R}(0) \cos \alpha_{\ell,R}(0) - v_R t \cos \eta_R}. \quad (36)$$

In (34), $\tau_\ell(t) = (D_{\ell,T}(t) + D_{\ell,R}(t))/c$ denotes the time-varying propagation delay from the center of the transmit antenna array to that of the receive array via the reflection of the ℓ-th cluster, where $D_{\ell,T}(t)$ is the real-time distance from the center of the transmit antenna array to the ℓ-th cluster, $D_{\ell,R}(t)$ is the real-time distance from the center of the receive antenna array to the ℓ-th cluster, which can be estimated as (37) and (38), respectively, as shown at the bottom of the page.

Furthermore, $\tau_{\ell,pq}(t) = (D_{\ell,p}(t) + D_{\ell,q}(t))/c$ denotes the time-varying propagation delay from the p-th transmit antenna to the q-th receive antenna via the reflection of the ℓ-th cluster,
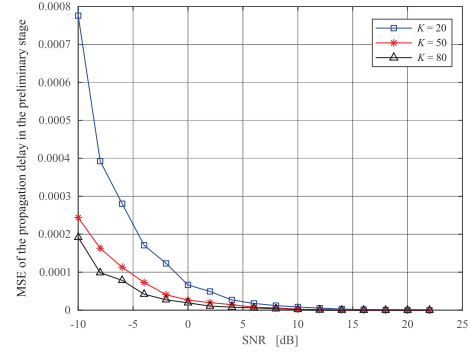

Fig. 3. MSEs performances of the propagation delay of the proposed channel model for the first tap with respect to the SNR when $D_0 = 100$ m, $M_T = M_R = 2$, and $\delta_T = \delta_R = \lambda/2$.
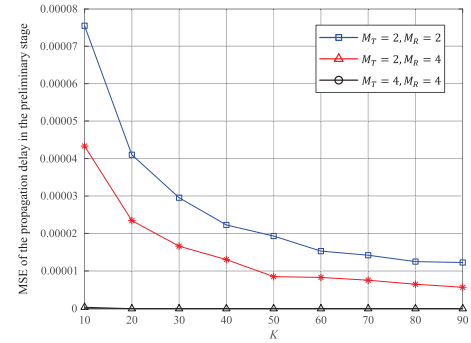

Fig. 4. MSEs performances of the propagation delay for the first tap with respect to the samples number K in different numbers of transmit/receive antennas when $D_0 = 100$ m, $K = 40$, $\delta_T = \delta_R = \lambda/2$, and SNR = 2 dB.

$D_{\ell,p}(t)$ and $D_{\ell,q}(t)$ are the real-time distances from the p-th transmit antenna and q-th receive antenna to the ℓ-th cluster, respectively, and they can be estimated as (39) and (40), respectively, as shown at the bottom of the page.

Overall, the procedure for generating the proposed channel model is shown as follows:

It is worth mentioning that the proposed channel model needs to know less channel information as compared to the standard channel models. Specifically, the standard models require not only the distance between the transceivers, but also the lengths of the major and semi-minor axes of the ellipse scattering channel model, etc., which cannot be assumed known in the real wireless communication scenarios. However, in this paper, we propose a Unitary matrix transformation algorithm to estimate the complex CIRs only based on the known distance between the MT and MR. The proposed algorithm can greatly improve the computational efficiency. It is also worth mentioning that the prior work mainly use MLE to estimate

$$\hat{D}_{\ell,T}(t) = \sqrt{\left(\hat{D}_{\ell,T}(0) \cos \hat{\alpha}_{\ell,T}(0) - v_T t \cos \eta_T\right)^2 + \left(\hat{D}_{\ell,T}(0) \sin \hat{\alpha}_{\ell,T}(0) - v_T t \sin \eta_T\right)^2}, \quad (37)$$

$$\hat{D}_{\ell,R}(t) = \sqrt{\left(\hat{D}_{\ell,R}(0) \cos \alpha_{\ell,R}(0) - v_R t \cos \eta_R\right)^2 + \left(\hat{D}_{\ell,R}(0) \sin \alpha_{\ell,R}(0) - v_R t \sin \eta_R\right)^2}. \quad (38)$$

$$\hat{D}_{\ell,p}(t) = \sqrt{\hat{D}_{\ell,T}^2(t) + \left(k_p \delta_T\right)^2 - 2\hat{D}_{\ell,T}(t) k_p \delta_T \cos\left(\hat{\alpha}_{\ell,T}(t) - \psi_T\right)}, \quad (39)$$

$$\hat{D}_{\ell,q}(t) = \sqrt{\hat{D}_{\ell,R}^2(t) + \left(k_q \delta_R\right)^2 - 2\hat{D}_{\ell,R}(t) k_q \delta_R \cos\left(\hat{\alpha}_{\ell,R}(t) - \psi_R\right)} \quad (40)$$
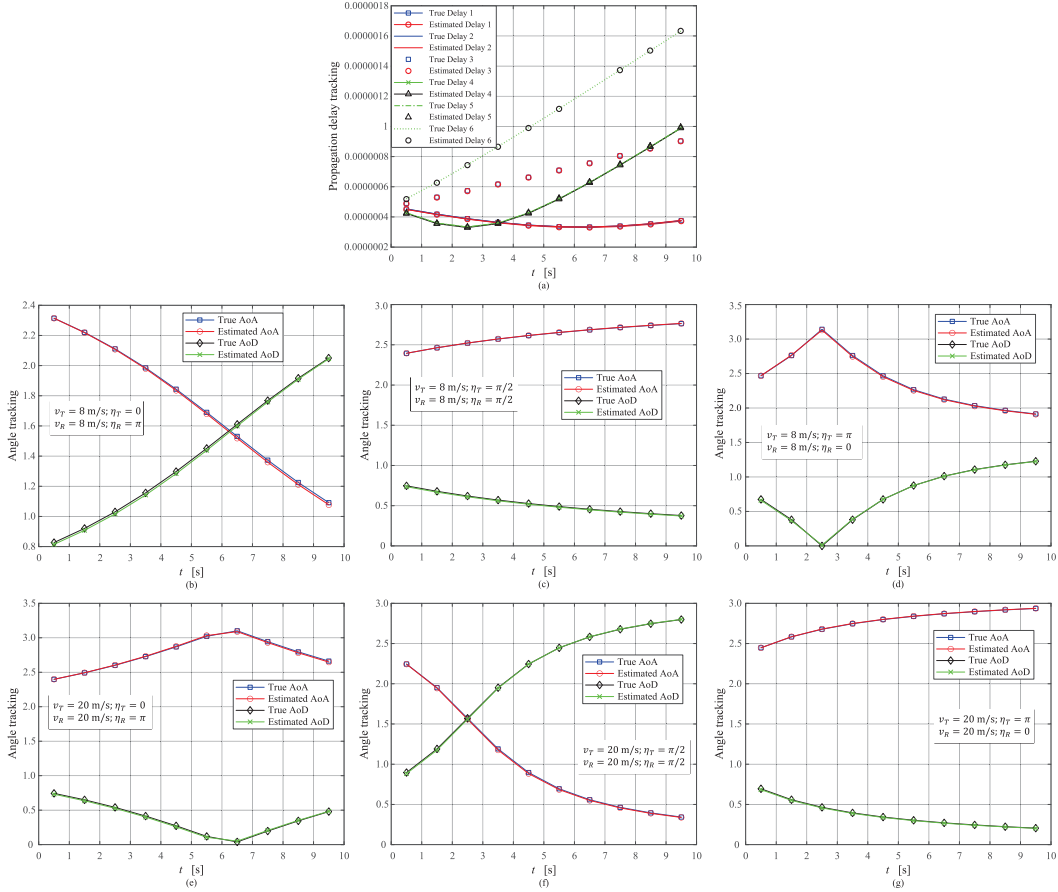
Fig. 5. Propagation delay and angle tracking in the real-time stage for the second tap when $D_0 = 100$ m, $M_T = M_R = 2$, $\delta_T = \delta_R = \lambda/2$, $K = 40$, and $\mathrm{SNR} = 0$ dB.

the parameters in wireless channels. However, in this paper, we estimate the lengths of the semi-major and semi-minor axes of the ellipse channel model for other taps by adopting the MLE to estimate the propagation delay $\hat{\tau}_1(0)$ for the first tap. Therefore, we can estimate the channel model in a real-time manner when the transmitter and receiver are both in motion.

IV. NUMERICAL RESULTS AND DISCUSSIONS

In this section, we study the performance of the proposed Unitary matrix estimation algorithm in the preliminary and real-time stages. Assume that the MT and MR are static during the initialization, i.e., $t = 0$, and hence the model parameters are constant during this time period. The transmitted signal of the p-th antenna is set to be a cosine signal, i.e., $s_p(\tau) = \cos(\tau)$, and the received noise variance is identical at all antennas, i.e., $\sigma_1^2 = \ldots = \sigma_q^2 = \ldots = \sigma_{M_R}^2 = \sigma^2$. The noise power σ^2 is derived as $\sigma^2 = P_s \times 10^{-\mathrm{SNR}/10}$, where P_s denotes the average power of the transmitted signal, which is defined as 1 in the following simulations. The SNR is the power ratio in dB of the transmitted signal to noise. It is worth mentioning that the clusters in the proposed channel model are all deterministic. When the waves emerging from the MT impinge on the different clusters before arriving at the MR, the propagation delays of the components are different. According to the V2V channel measurement campaigns in

[36] and [37], the resolution in delay is 100 ns. Therefore, we define the delay resolution between the taps is 100 ns in the proposed channel model [10]. It is also worth mentioning that the signal received at the receiver is a sum of the propagation rays with different delays (i.e., taps). However, in the estimation process of the preliminary stage, we only need a few samples of the propagation ray corresponding to the first tap, which can be acquired in practice in the following way. The receiver starts to record the signal once it appears and stop recording after a period shorter than the delay resolution between two different taps. As such, the recorded samples only come from the propagation ray corresponding to the first tap. In this case, we are able to estimate the propagation delay $\hat{\tau}_1(0)$ of the proposed channel model for the first tap.

A. Estimations of the Propagation Delay for the First Tap

To validate the statistical properties of the proposed channel model in the preliminary stage, some basic parameters are obtained by using $f_c = 5.9$ GHz, $\tau' = 100$ ns, $\varphi_0 = \pi/3$, $\psi_T = \psi_R = 2\pi/3$, $\alpha_{1,T}(0) = \pi/4$, and $\alpha_{1,R}(0) = 3\pi/4$. We adopt the mean squared error (MSE) to obtain the coarse propagation delay estimates. The MSE is an asymptically optimal estimator which generally performs very well even though the number of observation is not large. Define the
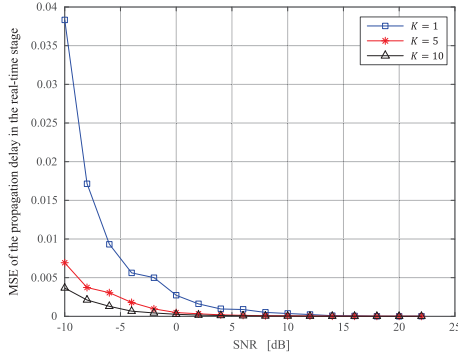
Fig. 6. MSEs performances of the propagation delay for the second tap with respect to the SNR in different numbers of discrete samples K when $D_0 = 100$ m, $M_T = M_R = 2$, $\delta_T = \delta_R = \lambda/2$, $v_T = 8$ m/s, $v_R = 10$ m/s, $\eta_T = 0$, $\eta_R = \pi$, and $t = 3$ s.
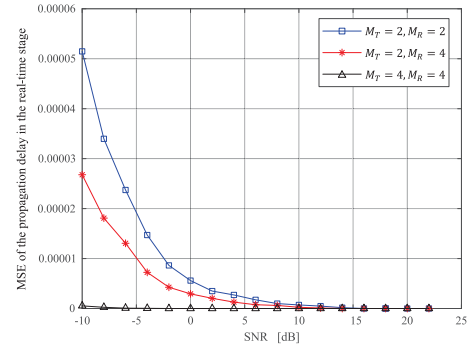

Fig. 7. MSEs performances of the propagation delay for the second tap with respect to the SNR in different numbers of transmit/receive antennas when $D_0 = 100$ m, $\delta_T = \delta_R = \lambda/2$, $K = 40$, $v_T = 15$ m/s, $v_R = 20$ m/s, $\eta_T = \pi$, $\eta_R = 0$, and $t = 3$ s.

expression of the MSE as [21]

$$\text{MSE} = \frac{1}{\mathcal{U}} \sum_{u=1}^{\mathcal{U}} \left[\frac{1}{\tau_1(0)}(\hat{\tau}_1(0) - \tau_1(0)) \right]^2, \tag{41}$$

where $\hat{\tau}_1(0)$ denotes the estimation of the propagation delay $\tau_1(0)$ of the u-th Monte Carlo trial. The total trial number is $\mathcal{U} = 400$. It can be seen from Fig. 3 and Fig. 4 that the estimation errors for estimating the propagation delay $\hat{\tau}_1(0)$ gradually decrease as the SNR or the number of samples K increases, which is in consistent with the simulation results in [38] and [39], thereby demonstrating that the estimation performance, such as the estimating precision, etc., can be very good for channel modeling, especially when the SNR or K is large.

Figure 4 shows the MSEs for estimating the propagation delay $\hat{\tau}_1(0)$ for different numbers of transmit/receive antennas in the preliminary stage. Note that the improvement of MSE performance caused by increasing of the antennas number can be interpreted by the diversity gain of MIMO system. As demonstrated in [40], when the transmitter and receiver are equipped with more antennas, the receiver is able to acquire more information on the propagation delay and achieve higher SNR, and hence obtain better estimation performance. Specifically, when the numbers of the transmit/receive antennas increase from $M_T = M_R = 2$ to $M_T = M_R = 4$, the MSEs decrease gradually, which agrees with the theoretical results in [41].

B. Estimations of the Delay and Angular Parameters for the Second Tap

To evaluate the propagation delay and angular parameters estimations in the real-time stage for the second tap, we conduct the real-time tracking of the MT and MR in different stages of motion in Fig. 5. Note that when the MT and MR move along the x-axis and get close to each other, i.e., $\eta_T = 0$ and $\eta_R = \pi$, the values of AoD tracking gradually increase as the moving time t increases, while the AoA tracking decrease slowly. However, when the MT and MR move along the x-axis and back to each other, i.e., $\eta_T = \pi$ and $\eta_R = 0$, the AoD tracking gradually decrease as the time t increases, while
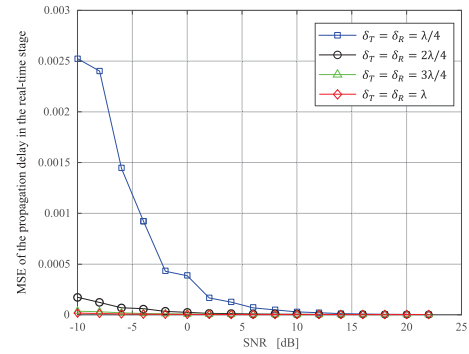

Fig. 8. MSEs performances of the propagation delay for the second tap with respect to the SNR in different antenna spacings of the transmit and receive arrays when $D_0 = 100$ m, $M_T = M_R = 2$, $K = 40$, $v_T = 10$ m/s, $v_R = 10$ m/s, $\eta_T = \eta_R = \pi/2$, and $t = 3$ s.
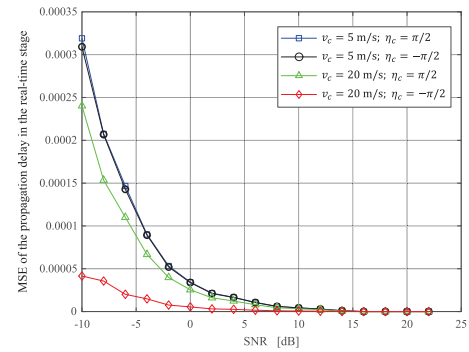

Fig. 9. MSEs performances of the propagation delay for the second tap with respect to moving direction/velocity of the cluster when when $D_0 = 100$ m, $\delta_T = \delta_R = \lambda/2$, $K = 40$, $v_T = v_R = 0$, $\eta_T = \pi$, $\eta_R = 0$, and $M_T = M_R = 2$.

the AoA tracking increases gradually, as shown in Fig. 5(c). Furthermore, we notice that when the MT and MR move perpendicular to the x-axis, i.e., $\eta_T = \pi/2$ and $\eta_R = \pi/2$, the AoD tracking firstly decrease to some value and then increases slowly as the time t increases, as shown in Fig. 5(b). Moreover, when the velocities of the transceivers increase from $v_T = v_R = 8$ m/s to $v_T = v_R = 20$ m/s, the AoD and AoA tracking vary more sufficiently small when t is small; however, as t increases, the AoD and AoA tracking tend to
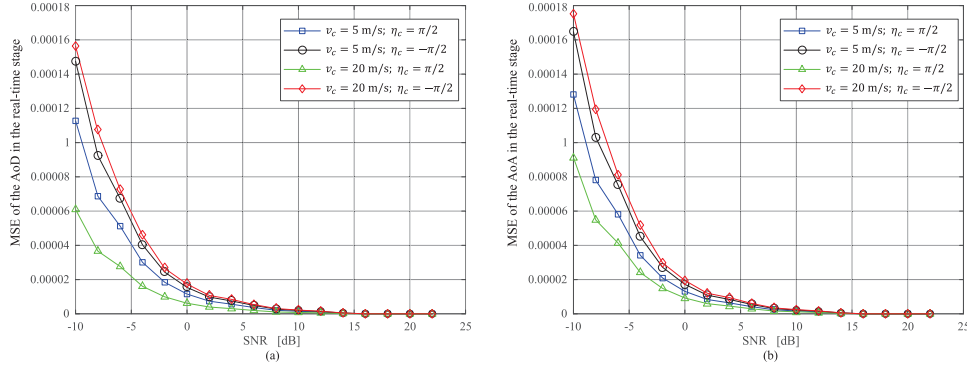
Fig. 10. MSEs performances of the AoD and AoA for the second tap in the real-time stage with respect to moving direction/velocity of the cluster when when $D_0 = 100$ m, $\delta_T = \delta_R = \lambda/2$, $K = 40$, $v_T = v_R = 0$, $\eta_T = \pi$, $\eta_R = 0$, $M_T = M_R = 2$, $and\, t = 2\ s$.

TABLE I

COMPARISONS OF THE SIMULATION TIME BETWEEN THE PROPOSED METHOD AND CONVENTIONAL METHOD

	Fig. 3	Fig. 4	Fig. 5	Fig. 6	Fig. 7	Fig. 8	Fig. 9	Fig. 10
Proposed Method	21min 31sec	27min 20sec	2min 13sec	3min 22sec	26min 49sec	16min 55sec	2min 31sec	6min 11sec
Conventional Method	29min 51sec	37min 25sec	2min 45sec	5min 37sec	40min 19sec	22min 40sec	2min 39sec	7min 56sec

be the same. Numerical results of the estimated propagation delay and AoD (or AoA) nicely match the true delay and AoD (or AoA), respectively, which verify that our derivations and analysis are accurate.

By setting $\ell = 2$ in (41), Fig. 6 shows the MSEs for estimating the propagation delay $\hat{\tau}_2(0)$ for the second tap with respect to the SNR for different numbers of the time samples K. It can be observed that when the parameter K increases from 1 to 10, the MSEs of the delay estimations decrease gradually.

Figure 7 shows the MSEs for estimating the propagation delay $\hat{\tau}_2(0)$ for different numbers of transmit/receive antennas. It can be seen that when the numbers of the transmit and receive antennas increase from $M_T = M_R = 2$ to $M_T = M_R = 4$, the MSEs of the propagation delay decrease gradually. The above observations are in agreement with the results in the preliminary stage in Fig. 4, which further demonstrate that the proposed algorithm is also applicable for wideband non-stationary channels in real-time stages and different taps.

Figure 8 shows the MSEs for estimating the propagation delay $\hat{\tau}_2(0)$ for different adjacent spacings of the transmit and receive antenna arrays. It can be observed that when the adjacent spacings of the transmit and receive antenna arrays increase from $\delta_T = \delta_R = \lambda/4$ to $\delta_T = \delta_R = \lambda$, the MSEs of the delay estimations decrease slowly.

To investigate the impacts of the moving velocities/directions of the cluster on the MSEs performances, we consider some specific moving directions of clusters in Fig. 9. Notice that when the cluster moves away from the x-axis, $\eta_c = \pi/2$, the MSEs for estimating the propagation delay $\hat{\tau}_2(0)$ in the case where $v_c = 5$ m/s is slightly larger than those where $v_c = 20$ m/s. Furthermore, when the cluster moves towards the x-axis, $\eta_c = -\pi/2$, the MSEs of

estimating the propagation delay in the case where $v_c = 5$ m/s is obviously smaller than those where $v_c = 20$ m/s. These results demonstrate that the proposed MSEs are related to the moving velocities/directions of the clusters in V2V channels.

Figure 10 shows the MSEs performances of the real-time AoD and AoA for the second tap. It can be seen that the MSEs for estimating the AoD are obviously lower than those for estimating the AoA. Note that when the moving velocity of the cluster increases from 5 m/s to 20 m/s, the AoD and AoA estimations have different characteristics as the cluster moves with different directions, which are in consistent with the results in Fig. 9.

Finally, by using the platform of MATLAB2020b with Intel(R) Core(TM) i5-4258U CPU @2.40GHz with 12 GB RAM, we compare the simulation time between the proposed method using the Unitary matrix transform algorithm and conventional one without the Unitary matrix transform in Table I. It can be seen that the simulation time of the proposed channel modeling method using Unitary matrix transform algorithm is obviously shorter than that of the conventional method without the Unitary matrix transform, which demonstrates the computational efficiency of the proposed channel modeling method.

V. CONCLUSION

In this paper, we have proposed a novel computationally efficient solution to investigate the characteristics of the proposed wideband MIMO V2V channel model for different propagation delays in different taps. By estimating the propagation delay of the proposed channel model for the first tap with a Unitary matrix transformation algorithm, we then estimate the MIMO V2V channel models for other taps. Furthermore, we have provided a solution to transform the closed-form

expressions of the complex CIRs into the real-domain using the Unitary transformation method.

It has been demonstrated that the MSEs performances for estimating the delay get better as the SNR increases; otherwise, the MSEs become worse. The MSEs are significantly affected by the moving direction/velocity/time of the MT, MR, and clusters. Numerical results of the estimated propagation delay nicely match the true delay, which verify that our derivations and analysis are accurate. Our research work therefore provides a new and efficient guidance for studying the statistical properties for different delays of B5G wideband non-stationary MIMO V2V wireless communication systems. As a part of future work, we consider developing better estimation algorithm for accurately estimating the model parameters in a noisy environment.

APPENDIX I

Let us first consider the number of the receive antenna elements as an even value, i.e., $M_R = 2\Lambda$, which indicates that the *left* Π-*real* matrix $\mathbf{Q}_{M_R K}$ can be derived in (15). In this case, the vectorized received sampling signal $\mathbf{y}$ can be partitioned into

$$\mathbf{y} = \begin{bmatrix} \mathbf{y}_{vec,1} \\ \mathbf{y}_{vec,2} \end{bmatrix} \in \mathbb{C}^{2\Lambda K \times 1}, \qquad (42)$$

where the block vectors $\mathbf{y}_{vec,1} = [\mathbf{y}_1, \mathbf{y}_2, \dots, \mathbf{y}_\Lambda]^T$ and $\mathbf{y}_{vec,2} = [\mathbf{y}_{\Lambda+1}, \mathbf{y}_{\Lambda+2}, \dots, \mathbf{y}_{2\Lambda}]^T$ are with the same size of $\Lambda K \times 1$. In substituting (42) into (19), the centro-Hermitian form of the vectorized discrete sampling received signal can be expressed as

$$\mathbf{Y}_{CH} = \begin{bmatrix} \mathbf{y}_{vec,1} & \mathbf{\Pi}_{\Lambda K} \mathbf{y}_{vec,2}^* \mathbf{\Pi}_1 \\ \mathbf{y}_{vec,2} & \mathbf{\Pi}_{\Lambda K} \mathbf{y}_{vec,1}^* \mathbf{\Pi}_1 \end{bmatrix}. \qquad (43)$$

By substituting (15) and (43) into (20), we can further express the real matrix $\mathbf{Y}_{Re} \in \mathbb{R}^{2\Lambda K \times 2}$ as (44), as shown at the bottom of the page, where $\text{Re}\{\cdot\}$ and $\text{Im}\{\cdot\}$ denote the real and imaginary parts of the complex matrices, respectively.

However, when the number of the receive antenna elements is an odd value, i.e., $M_R = 2\Lambda + 1$, the *left* Π-*real* matrix $\mathbf{Q}_{M_R K}$ can be derived for different number K of the samples. To be specific, we notice that $M_R K$ is an even value if the number of the discrete samples K is an even value,

i.e., $K = 2g$. In this case, we can partition the complex received signal vector $\mathbf{y}$ into the following expression:

$$\mathbf{y} = \begin{bmatrix} \mathbf{y}_{vec,1'} \\ \mathbf{y}_{vec,2'} \end{bmatrix} \in \mathbb{C}^{(2\Lambda+1)2g \times 1}, \qquad (45)$$

where $\mathbf{y}_{vec,1'} = [\mathbf{y}_1, \mathbf{y}_2, \dots, \mathbf{y}_\Lambda, \mathbf{y}_{\Lambda+1}(1:g)]^T$ and $\mathbf{y}_{vec,2'} = [\mathbf{y}_{\Lambda+1}((g+1):2g), \mathbf{y}_{\Lambda+2}, \dots, \mathbf{y}_{2\Lambda+1}]^T$ denote the block vectors with size $(2g\Lambda + g) \times 1$. In addition, $\mathbf{y}_{\Lambda+1}(1:g)$ and $\mathbf{y}_{\Lambda+1}((g+1):2g)$ are the first g and the last g received discrete samples of the $(\Lambda + 1)$-th antenna, respectively.

It is worth mentioning that when the M_R is an odd value, the corresponding real form of the vectorized sampling signal $\mathbf{y}$, which has a similar form as (44), can be expressed as (46), as shown at the bottom of the page.

It is worth mentioning that $M_R K$ is an odd value if the number of the samples K is an odd value, i.e., $K = 2g+1$; and hence the $\mathbf{Q}_{M_R K}$ can be chosen in (16). Here, the vectorized complex received signal vector $\mathbf{y}$ should be partitioned into another form, which can be expressed as

$$\mathbf{y} = \begin{bmatrix} \mathbf{y}_{vec,1''} \\ \mathbf{y}_{\Lambda+1}(g+1) \\ \mathbf{y}_{vec,2''} \end{bmatrix} \in \mathbb{C}^{(2\Lambda+1)(2g+1) \times 1}, \qquad (47)$$

where $\mathbf{y}_{vec,1''} = [\mathbf{y}_1, \mathbf{y}_2, \dots, \mathbf{y}_\Lambda, \mathbf{y}_{\Lambda+1}(1:g)]^T$ and $\mathbf{y}_{vec,2''} = [\mathbf{y}_{\Lambda+1}((g+2):(2g+1)), \mathbf{y}_{\Lambda+2}, \dots, \mathbf{y}_{2\Lambda+1}]^T$ are the block vectors with size $((2g+1)\Lambda + g) \times 1$; $\mathbf{y}_{\Lambda+1}(1:g)$ and $\mathbf{y}_{\Lambda+1}((g+2):(2g+1))$ denote the first g and the last g received samples of the $(\Lambda + 1)$-th antenna, respectively. Furthermore, $\mathbf{y}_{\Lambda+1}(g+1)$ is the $(g+1)$-th received sample of the $(\Lambda + 1)$-th antenna. Therefore, the centro-Hermitian form of the vectorized discrete sampling received signal can be expressed as

$$\mathbf{Y}_{CH} = \begin{bmatrix} \mathbf{y}_{vec,1''} & \mathbf{\Pi}_{(2g+1)\Lambda+g} \mathbf{y}_{vec,2''}^* \mathbf{\Pi}_1 \\ \mathbf{y}_{\Lambda+1}(g+1) & \mathbf{y}_{\Lambda+1}^*(g+1) \\ \mathbf{y}_{vec,2''} & \mathbf{\Pi}_{(2g+1)\Lambda+g} \mathbf{y}_{vec,1''}^* \mathbf{\Pi}_1 \end{bmatrix}. \qquad (48)$$

By substituting (16) and (48) into (20), the real form matrix of the sample vector $\mathbf{y}$ for the case of $M_R = 2\Lambda + 1$ and $K = 2g + 1$ can be expressed as (49), as shown at the bottom of the next page.

In the following part, we just consider that the number of the receive antenna elements is an even value, i.e., $M_R = 2\Lambda$. For the case of $M_R = 2\Lambda + 1$, the discussion can be derived in a similar way and we omit it for brevity. In this

$$\begin{aligned} \mathbf{Y}_{Re} &= \frac{1}{\sqrt{2}} \begin{bmatrix} \mathbf{I}_{\Lambda K} & \mathbf{\Pi}_{\Lambda K} \\ -j\mathbf{I}_{\Lambda K} & j\mathbf{\Pi}_{\Lambda K} \end{bmatrix} \begin{bmatrix} \mathbf{y}_{vec,1} & \mathbf{\Pi}_{\Lambda K} \mathbf{y}_{vec,2}^* \mathbf{\Pi}_1 \\ \mathbf{y}_{vec,2} & \mathbf{\Pi}_{\Lambda K} \mathbf{y}_{vec,1}^* \mathbf{\Pi}_1 \end{bmatrix} \frac{1}{\sqrt{2}} \begin{bmatrix} \mathbf{I}_1 & j\mathbf{I}_1 \\ \mathbf{\Pi}_1 & -j\mathbf{\Pi}_1 \end{bmatrix} \\ &= \frac{1}{2} \begin{bmatrix} \mathbf{y}_{vec,1} + \mathbf{y}_{vec,1}^* + \mathbf{\Pi}_{\Lambda K}(\mathbf{y}_{vec,2} + \mathbf{y}_{vec,2}^*) & j\big[(\mathbf{y}_{vec,1} - \mathbf{y}_{vec,1}^*) + \mathbf{\Pi}_{\Lambda K}(\mathbf{y}_{vec,2} - \mathbf{y}_{vec,2}^*)\big] \\ j\big[(\mathbf{y}_{vec,1}^* - \mathbf{y}_{vec,1}) + \mathbf{\Pi}_{\Lambda K}(\mathbf{y}_{vec,2} - \mathbf{y}_{vec,2}^*)\big] & \mathbf{y}_{vec,1} + \mathbf{y}_{vec,1}^* - \mathbf{\Pi}_{\Lambda K}(\mathbf{y}_{vec,2} + \mathbf{y}_{vec,2}^*) \end{bmatrix} \\ &= \begin{bmatrix} \text{Re}\{\mathbf{y}_{vec,1} + \mathbf{\Pi}_{\Lambda K} \mathbf{y}_{vec,2}\} & -\text{Im}\{\mathbf{y}_{vec,1} + \mathbf{\Pi}_{\Lambda K} \mathbf{y}_{vec,2}\} \\ \text{Im}\{\mathbf{y}_{vec,1} - \mathbf{\Pi}_{\Lambda K} \mathbf{y}_{vec,2}\} & \text{Re}\{\mathbf{y}_{vec,1} - \mathbf{\Pi}_{\Lambda K} \mathbf{y}_{vec,2}\} \end{bmatrix}, \end{aligned} \qquad (44)$$

$$\begin{aligned} \mathbf{Y}_{Re} &= \mathbf{Q}_{(2\Lambda+1)2g}^H \begin{bmatrix} \mathbf{y} & \mathbf{\Pi}_{(2\Lambda+1)2g} \mathbf{y}^* \end{bmatrix} \begin{bmatrix} \mathbf{I}_1 & \\ & \mathbf{\Pi}_1 \end{bmatrix} \mathbf{Q}_2 \\ &= \begin{bmatrix} \text{Re}\{\mathbf{y}_{vec,1'} + \mathbf{\Pi}_{2g\Lambda+g} \mathbf{y}_{vec,2'}\} & -\text{Im}\{\mathbf{y}_{vec,1'} + \mathbf{\Pi}_{2g\Lambda+g} \mathbf{y}_{vec,2'}\} \\ \text{Im}\{\mathbf{y}_{vec,1'} - \mathbf{\Pi}_{2g\Lambda+g} \mathbf{y}_{vec,2'}\} & \text{Re}\{\mathbf{y}_{vec,1'} - \mathbf{\Pi}_{2g\Lambda+g} \mathbf{y}_{vec,2'}\} \end{bmatrix}. \end{aligned} \qquad (46)$$

case, the partitioned term $\mathbf{y}_{vec,1} + \mathbf{\Pi}_{\Lambda K}\mathbf{y}_{vec,2}$ in (44) can be expressed as

$$
\mathbf{y}_{vec,1} + \mathbf{\Pi}_{\Lambda K}\mathbf{y}_{vec,2} =
\begin{bmatrix}
\mathbf{y}_1^T + \mathbf{\Pi}_K\mathbf{y}_{2\Lambda}^T \\
\mathbf{y}_2^T + \mathbf{\Pi}_K\mathbf{y}_{2\Lambda-1}^T \\
\vdots \\
\mathbf{y}_\zeta^T + \mathbf{\Pi}_K\mathbf{y}_{2\Lambda-\zeta+1}^T \\
\vdots \\
\mathbf{y}_\Lambda^T + \mathbf{\Pi}_K\mathbf{y}_{\Lambda+1}^T
\end{bmatrix},
\quad (50)
$$

where the ζ-th ($\zeta = 1, 2, \ldots, \Lambda$) term can be written as (51), as shown at the bottom of the page.

By substituting the expression of the discrete received signal into (51), we can obtain (52), as shown at the bottom of the page. where $\tau_{\ell,p\zeta}(0)$ and $\tau_{\ell,p(2\Lambda-\zeta+1)}(0)$ are the propagation delays of the NLoS propagation components, respectively. The $\mathbf{y}_{vec,1} + \mathbf{\Pi}_{\Lambda K}\mathbf{y}_{vec,2}$ is a $\Lambda K \times 1$ dimensional column vector, and hence the ζ-th term of the $\mathbf{y}_{vec,1} + \mathbf{\Pi}_{\Lambda K}\mathbf{y}_{vec,2}$ is simply the combination of the received sampling signals received at the ζ-th and the $(2\Lambda-\zeta+1)$-th antennas. It is worth mentioning that the expression of the partitioned term $\mathbf{y}_{vec,1} - \mathbf{\Pi}_{\Lambda K}\mathbf{y}_{vec,2}$ can be derived in a similar method.

Define κ ($\kappa = 1, 2, \ldots, \Lambda$), which has a similar meaning as ζ in (50), as the received sample vector index of the partitioned vectors in (44) for the case of $M_R = 2\Lambda$. As demonstrated in [42], the mean value of the k-th element of the κ-th sample vector in the partitioned vector $\mathrm{Re}\{\mathbf{y}_{vec,1} + \mathbf{\Pi}_{\Lambda K}\mathbf{y}_{vec,2}\}$ is

denoted by $\boldsymbol{\mu}_{1,\kappa}(k)$, which can be expressed as

$$
\boldsymbol{\mu}_{1,\kappa}(k) = \sum_{p=1}^{M_T} \chi_1 s_p\big(kT_0 - \tau_1(0)\big) \cos\big(\varphi_0 - 2\pi f_c \tau_{1,p\kappa}(0)\big)
$$
$$
+ \sum_{p=1}^{M_T} \chi_1 s_p\big((K - k + 1)T_0 - \tau_1(0)\big)
$$
$$
\times \cos\big(\varphi_0 - 2\pi f_c \tau_{1,p(2\Lambda-\kappa+1)}(0)\big). \quad (53)
$$

Moreover, the mean value of the k-th element of the κ-th sample vector in the partitioned vector $-\mathrm{Im}\{\mathbf{y}_{vec,1} + \mathbf{\Pi}_{\Lambda K}\mathbf{y}_{vec,2}\}$ is denoted by $\boldsymbol{\mu}_{2,\kappa}(k)$, being expressed as

$$
\boldsymbol{\mu}_{2,\kappa}(k) = -\sum_{p=1}^{M_T} \chi_1 s_p\big(kT_0 - \tau_1(0)\big) \sin\big(\varphi_0 - 2\pi f_c \tau_{1,p\kappa}(0)\big)
$$
$$
- \sum_{p=1}^{M_T} \chi_1 s_p\big((K - k + 1)T_0 - \tau_1(0)\big)
$$
$$
\times \sin\big(\varphi_0 - 2\pi f_c \tau_{1,p(2\Lambda-\kappa+1)}(0)\big). \quad (54)
$$

Denote the mean values of the k-th elements of the κ-th sample vector in the partitioned vectors $\mathrm{Im}\{\mathbf{y}_{vec,1} - \mathbf{\Pi}_{\Lambda K}\mathbf{y}_{vec,2}\}$ and $\mathrm{Re}\{\mathbf{y}_{vec,1} - \mathbf{\Pi}_{\Lambda K}\mathbf{y}_{vec,2}\}$ as $\boldsymbol{\mu}_{3,\kappa}(k)$ and $\boldsymbol{\mu}_{4,\kappa}(k)$, respectively, which can be derived in a similar method, we omit them here for brevity.

$$
\mathbf{Y}_{Re} = \frac{1}{\sqrt{2}}
\begin{bmatrix}
\mathbf{I}_{(2g+1)\Lambda+g} & \mathbf{0}_{(2g+1)\Lambda+g} & \mathbf{\Pi}_{(2g+1)\Lambda+g} \\
\mathbf{0}_{(2g+1)\Lambda+g}^T & \sqrt{2} & \mathbf{0}_{(2g+1)\Lambda+g}^T \\
-j\mathbf{I}_{(2g+1)\Lambda+g} & \mathbf{0}_{(2g+1)\Lambda+g} & j\mathbf{\Pi}_{(2g+1)\Lambda+g}
\end{bmatrix}
\times
\begin{bmatrix}
\mathbf{y}_{vec,1''} & \mathbf{\Pi}_{(2g+1)\Lambda+g}\mathbf{y}_{vec,2''}^*\mathbf{\Pi}_1 \\
\mathbf{y}_{\Lambda+1}(g+1) & \mathbf{y}_{(2g+1)\Lambda+g}^* \\
\mathbf{y}_{vec,2''} & \mathbf{\Pi}_{(2g+1)\Lambda+g}\mathbf{y}_{vec,1''}^*\mathbf{\Pi}_1
\end{bmatrix}
\times \frac{1}{\sqrt{2}}
\begin{bmatrix}
\mathbf{I}_1 & j\mathbf{I}_1 \\
\mathbf{\Pi}_1 & -j\mathbf{\Pi}_1
\end{bmatrix}
$$
$$
=
\begin{bmatrix}
\mathrm{Re}\{\mathbf{y}_{vec,1''} + \mathbf{\Pi}_{(2g+1)\Lambda+g}\mathbf{y}_{vec,2''}\} & -\mathrm{Im}\{\mathbf{y}_{vec,1''} + \mathbf{\Pi}_{(2g+1)\Lambda+g}\mathbf{y}_{vec,2''}\} \\
\sqrt{2}\,\mathrm{Re}\{\mathbf{y}_{\Lambda+1}(g+1)\} & -\sqrt{2}\,\mathrm{Im}\{\mathbf{y}_{\Lambda+1}(g+1)\} \\
\mathrm{Im}\{\mathbf{y}_{vec,1''} - \mathbf{\Pi}_{(2g+1)\Lambda+g}\mathbf{y}_{vec,2''}\} & \mathrm{Re}\{\mathbf{y}_{vec,1''} - \mathbf{\Pi}_{(2g+1)\Lambda+g}\mathbf{y}_{vec,2''}\}
\end{bmatrix}. \quad (49)
$$

$$
\mathbf{y}_\zeta^T + \mathbf{\Pi}_K\mathbf{y}_{2\Lambda-\zeta+1}^T = \Big[\, y_\zeta(1T_0), \ldots, y_\zeta(kT_0), \ldots, y_\zeta(KT_0) \,\Big]^T
$$
$$
+ \Big[\, y_{2\Lambda-\zeta+1}(KT_0), \ldots, y_{2\Lambda-\zeta+1}((K-k+1)T_0), \ldots, y_{2\Lambda-\zeta+1}(1T_0) \,\Big]^T. \quad (51)
$$

$$
\mathbf{y}_\zeta^T + \mathbf{\Pi}_K\mathbf{y}_{2\Lambda-\zeta+1}^T = \sum_{p=1}^{M_T} \left(\chi_1 \, e^{j\big(\varphi_0 - 2\pi f_c \tau_{1,p\zeta}(0)\big)}
\begin{bmatrix}
s_p\big(1T_0 - \tau_1(0)\big) \\
s_p\big(2T_0 - \tau_1(0)\big) \\
\vdots \\
s_p\big(kT_0 - \tau_1(0)\big) \\
\vdots \\
s_p\big(KT_0 - \tau_1(0)\big)
\end{bmatrix}
\right.
$$
$$
\left.
+ e^{j\big(\varphi_0 - 2\pi f_c \tau_{1,p(2\Lambda-\zeta+1)}(0)\big)}
\begin{bmatrix}
s_p\big(KT_0 - \tau_1(0)\big) \\
s_p\big((K-1)T_0 - \tau_1(0)\big) \\
\vdots \\
s_p\big((K-k+1)T_0 - \tau_1(0)\big) \\
\vdots \\
s_p\big(1T_0 - \tau_1(0)\big)
\end{bmatrix}
\right)
+
\begin{bmatrix}
n_\zeta(1T_0) + n_{2\Lambda-\zeta+1}(KT_0) \\
n_\zeta(2T_0) + n_{2\Lambda-\zeta+1}((K-1)T_0) \\
\vdots \\
n_\zeta(kT_0) + n_{2\Lambda-\zeta+1}((K-k+1)T_0) \\
\vdots \\
n_\zeta(KT_0) + n_{2\Lambda-\zeta+1}(1T_0)
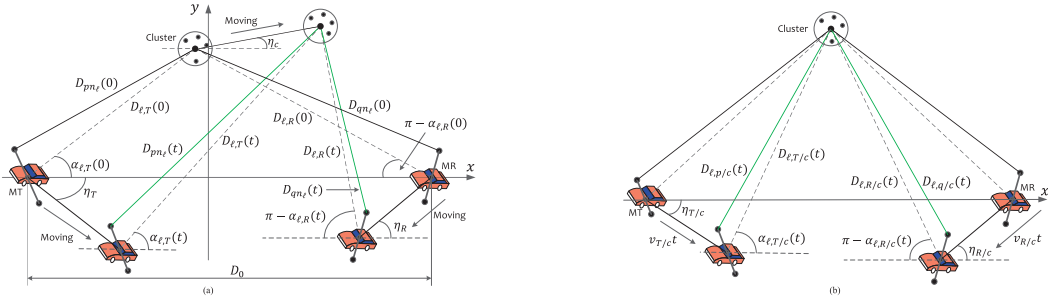\end{bmatrix}
\quad (52)
$$

Fig. 11. Diagrams of MIMO V2V channel models: (a) geometric relations in V2V channels (b) geometric update of V2V channels.

Finally, the $2\Lambda K \times 2$ dimensional real matrix $\mathbf{Y}_{Re}$ in (44) can be vectorized to a $4\Lambda K \times 1$ dimensional column vector as follows:

$$\mathbf{y}_{Re} = \begin{bmatrix} \mathrm{Re}\{\mathbf{y}_{vec,1} + \boldsymbol{\Pi}_{\Lambda K}\mathbf{y}_{vec,2}\} \\ -\mathrm{Im}\{\mathbf{y}_{vec,1} + \boldsymbol{\Pi}_{\Lambda K}\mathbf{y}_{vec,2}\} \\ \mathrm{Im}\{\mathbf{y}_{vec,1} - \boldsymbol{\Pi}_{\Lambda K}\mathbf{y}_{vec,2}\} \\ \mathrm{Re}\{\mathbf{y}_{vec,1} - \boldsymbol{\Pi}_{\Lambda K}\mathbf{y}_{vec,2}\} \end{bmatrix}. \quad (55)$$

APPENDIX II

Let us consider a more general V2V communication scenario, as shown in Fig. 11(a), where MT, MR, and clusters are all in motion. We define v_c and η_c as the moving velocity and direction of the cluster, respectively. In the following, we consider the moving cluster as the reference point, as in Fig. 11(b). Then, the distances from the centers of the transmit and receive antenna arrays to the ℓ-th moving cluster can be respectively expressed as

$$D_{\ell,T/c}(t)$$
$$= \Big[\big(D_{\ell,T}(0)\sin\alpha_{\ell,T}(0) - v_T t \sin\eta_T - v_c t \sin\eta_c\big)^2$$
$$+ \big(D_{\ell,T}(0)\cos\alpha_{\ell,T}(0) - v_T t \cos\eta_T - v_c t \cos\eta_c\big)^2\Big]^{1/2}, \quad (56)$$

$$D_{\ell,R/c}(t)$$
$$= \Big[\big(D_{\ell,R}(0)\sin\alpha_{\ell,R}(0) - v_R t \sin\eta_R - v_c t \sin\eta_c\big)^2$$
$$+ \big(D_{\ell,R}(0)\cos\alpha_{\ell,R}(0) - v_R t \cos\eta_R - v_c t \cos\eta_c\big)^2\Big]^{1/2}. \quad (57)$$

By substituting (56) and (57) into (39) and (40), respectively, the distances from the p-th transmit antenna and q-th receive antenna to the ℓ-th moving cluster, denoted by $D_{\ell,p/c}(t)$ and $D_{\ell,q/c}(t)$, can be obtained. In this case, the complex channel response for the NLoS propagation rays for other taps ($\ell > 1$) can be expressed as

$$h_{\ell,pq}(t) = e^{j\big(\varphi_0 - 2\pi f_c\big(D_{\ell,p/c}(t) + D_{\ell,q/c}(t)\big)/c\big)}$$
$$\times e^{j\frac{2\pi}{\lambda}v_{T/s}t\cos\big(\alpha_{\ell,T/c}(t) - \eta_{T/s}\big)}$$
$$\times e^{j\frac{2\pi}{\lambda}v_{R/s}t\cos\big(\alpha_{\ell,R/c}(t) - \eta_{R/s}\big)}, \quad (58)$$

where $v_{T/c}$ and $v_{R/c}$ denote the moving velocities of the MT and MR relative to the moving clusters, respectively, which

can be expressed as

$$v_{T/c}$$
$$= \sqrt{\big(v_T \cos\eta_T - v_c \cos\eta_c\big)^2 + \big(v_T \sin\eta_T - v_c \sin\eta_c\big)^2}, \quad (59)$$

$$v_{R/c}$$
$$= \sqrt{\big(v_R \cos\eta_R - v_c \cos\eta_c\big)^2 + \big(v_R \sin\eta_R - v_c \sin\eta_c\big)^2}. \quad (60)$$

Furthermore, $\eta_{T/s}$ and $\eta_{R/s}$ are the moving directions of the MT and MR relative to the moving clusters, respectively. We have that

$$\eta_{T/s} = \arctan\frac{v_T \sin\eta_T - v_c \sin\eta_c}{v_T \cos\eta_T - v_c \cos\eta_c}, \quad (61)$$

$$\eta_{R/s} = \arctan\frac{v_R \sin\eta_R - v_c \sin\eta_c}{v_R \cos\eta_R - v_c \cos\eta_c}. \quad (62)$$

In addition, $\alpha_{\ell,T/c}(t)$ and $\alpha_{\ell,R/c}(t)$ are the real-time AoD and AoA, respectively, which can be expressed as

$$\alpha_{\ell,T/c}(t)$$
$$= \arctan\frac{D_{\ell,T}(0)\sin\alpha_{\ell,T}(0) - v_T t \sin\eta_T + v_c t \sin\eta_c}{D_{\ell,T}(0)\cos\alpha_{\ell,T}(0) - v_T t \cos\eta_T + v_c t \cos\eta_c}, \quad (63)$$

$$\alpha_{\ell,R/c}(t)$$
$$= \arctan\frac{D_{\ell,R}(0)\sin\alpha_{\ell,R}(0) - v_R t \sin\eta_R + v_c t \sin\eta_c}{D_{\ell,R}(0)\cos\alpha_{\ell,R}(0) - v_R t \cos\eta_R + v_c t \cos\eta_c}. \quad (64)$$

REFERENCES

[1] S. Hong *et al.*, "Applications of self-interference cancellation in 5G and beyond," *IEEE Commun. Mag.*, vol. 52, no. 2, pp. 114–121, Feb. 2014.

[2] R. He *et al.*, "Propagation channels of 5G millimeter-wave vehicle-to-vehicle communications: Recent advances and future challenges," *IEEE Veh. Technol. Mag.*, vol. 15, no. 1, pp. 16–26, Mar. 2020.

[3] H. Jiang, M. Mukherjee, J. Zhou, and J. Lloret, "Channel modeling and characteristics for 6G wireless communications," *IEEE Netw.*, vol. 35, no. 1, pp. 296–303, Jan. 2021, doi: 10.1109/MNET.011.2000348.

[4] H. Jiang, Z. Zhang, J. Dang, and L. Wu, "Analysis of geometric multibounced virtual scattering channel model for dense urban street environments," *IEEE Trans. Veh. Technol.*, vol. 66, no. 3, pp. 1903–1912, Mar. 2017.

[5] X. Cheng, C.-X. Wang, D. Laurenson, S. Salous, and A. Vasilakos, "An adaptive geometry-based stochastic model for non-isotropic MIMO mobile-to-mobile channels," *IEEE Trans. Wireless Commun.*, vol. 8, no. 9, pp. 4824–4835, Sep. 2009.

[6] R. He, B. Ai, G. L. Stuber, and Z. Zhong, "Mobility model-based non-stationary mobile-to-mobile channel modeling," *IEEE Trans. Wireless Commun.*, vol. 17, no. 7, pp. 4388–4400, Jul. 2018.

[7] H. Jiang, Z. Zhang, and G. Gui, "Three-dimensional non-stationary wideband geometry-based UAV channel model for A2G communication environments," *IEEE Access*, vol. 7, pp. 26116–26122, Feb. 2019.

[8] X. Cheng, Q. Yao, M. Wen, C.-X. Wang, L.-Y. Song, and B.-L. Jiao, "Wideband channel modeling and intercarrier interference cancellation for vehicle-to-vehicle communication systems," *IEEE J. Sel. Areas Commun.*, vol. 31, no. 9, pp. 434–448, Sep. 2013.

[9] H. Jiang, Z. Zhang, L. Wu, J. Dang, and G. Gui, "A 3-D non-stationary wideband geometry-based channel model for MIMO vehicle-to-vehicle communications in tunnel environments," *IEEE Trans. Veh. Technol.*, vol. 68, no. 7, pp. 6257–6271, Jul. 2019.

[10] Y. Yuan, C.-X. Wang, Y. He, M. M. Alwakeel, and E.-H.-M. Aggoune, "3D wideband non-stationary geometry-based stochastic models for non-isotropic MIMO vehicle-to-vehicle channels," *IEEE Trans. Wireless Commun.*, vol. 14, no. 12, pp. 6883–6895, Dec. 2015.

[11] C. Xiao, J. Wu, S.-Y. Leong, Y. R. Zheng, and K. B. Letaief, "A discrete-time model for triply selective MIMO Rayleigh fading channels," *IEEE Trans. Wireless Commun.*, vol. 3, no. 5, pp. 1678–1688, Sep. 2004.

[12] C. Xiao, Y. Zheng, and N. Beaulieu, "Novel sum-of-sinusoids simulation models for Rayleigh and Rician fading channels," *IEEE Trans. Wireless Commun.*, vol. 5, no. 12, pp. 3667–3679, Dec. 2006.

[13] K.-C. Huarng and C.-C. Yeh, "A unitary transformation method for angle-of-arrival estimation," *IEEE Trans. Signal Process.*, vol. 39, no. 4, pp. 975–977, Apr. 1991.

[14] M. Johnny, M. R. Aref, and F. Razzazi, "Effect of unitary transformation on Bayesian information criterion for source numbering in array processing," *IET Signal Process.*, vol. 13, no. 7, pp. 670–678, Sep. 2019.

[15] H. Jiang, Z. Zhang, and G. Gui, "A novel estimated wideband geometry-based vehicle-to-vehicle channel model using an AoD and AoA estimation algorithm," *IEEE Access*, vol. 7, pp. 35124–35131, Feb. 2019.

[16] D. Xu, Z. Liu, Y. Xu, and J. Cao, "A unitary transformation method for DOA estimation with uniform circular array," in *Proc. IEEE WCNIS*, Beijing, China, Jun. 2010, pp. 142–145.

[17] M. Yang *et al.*, "A cluster-based three-dimensional channel model for vehicle-to-vehicle communications," *IEEE Trans. Veh. Technol.*, vol. 68, no. 6, pp. 5208–5220, Jun. 2019.

[18] A. Ghazal *et al.*, "A non-stationary IMT-advanced MIMO channel model for high-mobility wireless communication systems," *IEEE Trans. Wireless Commun.*, vol. 16, no. 4, pp. 2057–2068, Apr. 2017.

[19] H. Jiang, Z. Zhang, J. Dang, and L. Wu, "A novel 3-D massive MIMO channel model for vehicle-to-vehicle communication environments," *IEEE Trans. Commun.*, vol. 66, no. 1, pp. 79–90, Jan. 2018.

[20] R. He, B. Ai, G. L. Stuber, G. Wang, and Z. Zhong, "Geometrical-based modeling for millimeter-wave MIMO mobile-to-mobile channels," *IEEE Trans. Veh. Technol.*, vol. 67, no. 4, pp. 2848–2863, Apr. 2018.

[21] M. S. Kay, *Fundamentals of Statistical Processing: Estimation Theory*, vol. 1. Upper Saddle River, NJ, USA: Prentice-Hall, 1993.

[22] Q. Qin, L. Gui, P. Cheng, and B. Gong, "Time-varying channel estimation for millimeter wave multiuser MIMO systems," *IEEE Trans. Veh. Technol.*, vol. 67, no. 10, pp. 9435–9448, Oct. 2018.

[23] F.-G. Yan, S. Liu, J. Wang, M. Jin, and Y. Shen, "Unitary direction of arrival estimation based on a second forward/backward averaging technique," *IEEE Commun. Lett.*, vol. 22, no. 3, pp. 554–557, Mar. 2018.

[24] A. Lee, "Centrohermitian and skew-centrohermitian matrices," *Linear Algebra Appl.*, vol. 29, pp. 205–210, Feb. 1980.

[25] A. A. Kalachikov and N. S. Shelkunov, "Construction and validation of analytical wireless MIMO channel models based on channel measurement data," in *Proc. APEIE*, Novosibirsk, Russia, 2018, pp. 175–179.

[26] T. E. Abrudan, J. Eriksson, and V. Koivunen, "Steepest descent algorithms for optimization under unitary matrix constraint," *IEEE Trans. Signal Process.*, vol. 56, no. 3, pp. 1134–1147, Mar. 2008.

[27] J. Li, D. Li, D. Jiang, and X. Zhang, "Extended-aperture unitary root MUSIC-based DOA estimation for coprime array," *IEEE Commun. Lett.*, vol. 22, no. 4, pp. 752–755, Apr. 2018.

[28] L. Xu, F. Wen, and X. Zhang, "A novel unitary PARAFAC algorithm for joint DOA and frequency estimation," *IEEE Commun. Lett.*, vol. 23, no. 4, pp. 660–663, Apr. 2019.

[29] M. Haardt and J. A. Nossek, "Unitary ESPRIT: How to obtain increased estimation accuracy with a reduced computational burden," *IEEE Trans. Signal Process.*, vol. 43, no. 5, pp. 1232–1242, May 1995.

[30] A. L. Moustakas, S. H. Simon, and T. L. Marzetta, "Capacity of differential versus nondifferential unitary space–time modulation for MIMO channels," *IEEE Trans. Inf. Theory*, vol. 52, no. 8, pp. 3622–3634, Aug. 2006.

[31] M. Protter, I. Yavneh, and M. Elad, "Closed-form MMSE estimation for signal denoising under sparse representation modeling over a unitary dictionary," *IEEE Trans. Signal Process.*, vol. 58, no. 7, pp. 3471–3484, Jul. 2010.

[32] L. Wan, K. Liu, Y.-C. Liang, and T. Zhu, "DOA and polarization estimation for non-circular signals in 3-D millimeter wave polarized massive MIMO systems," *IEEE Trans. Wireless Commun.*, early access, Jan. 8, 2021, doi: 10.1109/TWC.2020.3047866.

[33] R. Kumaresan and D. W. Tufts, "Estimating the angles of arrival of multiple plane waves," *IEEE Trans. Aerosp. Electron. Syst.*, vol. AES-19, no. 1, pp. 134–139, Jan. 1983.

[34] Z. M. Liu, C. W. Zhang, and P. S. Yu, "Directional-of-arrival estimation based on deep neural networks with robustness to array imperfections," *IEEE Trans. Antennas Propag.*, vol. 66, no. 12, pp. 7315–7327, Dec. 2018.

[35] C. Wu and J. Elangage, "Multiemitter two-dimensional angle-of-arrival estimator via compressive sensing," *IEEE Trans. Aerosp. Electron. Syst.*, vol. 56, no. 4, pp. 2884–2895, Aug. 2020.

[36] I. Sen and D. W. Matolak, "Vehicle–vehicle channel models for the 5-GHz band," *IEEE Trans. Intell. Transp. Syst.*, vol. 9, no. 2, pp. 235–245, Jun. 2008.

[37] G. Acosta-Marum and M. A. Ingram, "Six time- and frequency- selective empirical channel models for vehicular wireless LANs," *IEEE Veh. Technol. Mag.*, vol. 2, no. 4, pp. 4–11, Dec. 2007.

[38] T. Chen, L. Liu, and D. Pan, "A ULA-based MWC discrete compressed sampling structure for carrier frequency and AOA estimation," *IEEE Access*, vol. 5, pp. 14154–14164, Aug. 2017.

[39] L. S. Pillutla and R. Annavajjala, "Bayesian CRLB for joint AoA, AoD and multipath gain estimation in millimeter wave wireless networks," in *Proc. IEEE Global Commun. Conf. (GLOBECOM)*, Singapore, Dec. 2017, pp. 1–6.

[40] A. Goldsmith, *Wireless Communications*. Cambridge, U.K.: Cambridge Univ. Press, 2005.

[41] D. Zhu, J. Choi, and R. W. Heath, "Auxiliary beam pair enabled AoD and AoA estimation in closed-loop large-scale millimeter-wave MIMO systems," *IEEE Trans. Wireless Commun.*, vol. 16, no. 7, pp. 4770–4785, Jul. 2017.

[42] J. Li, D. Jiang, and X. Zhang, "DOA estimation based on combined unitary ESPRIT for coprime MIMO radar," *IEEE Commun. Lett.*, vol. 21, no. 1, pp. 96–99, Jan. 2017.

Hao Jiang (Member, IEEE) received the B.S. and M.S. degrees in electrical and information engineering from the Nanjing University of Information Science and Technology, Nanjing, China, in 2012 and 2015, respectively, and the Ph.D. degree from Southeast University, Nanjing, in 2019. From 2017 to 2018, he was a Visiting Student with the Department of Electrical Engineering, Columbia University in the City of New York, New York, USA. Since April 2019, he has been a Professor with the School of Information Science and Engineering, Nanjing University of Information Science and Technology. His current research interests include wireless channel measurements and modeling, B5G wireless communication networks, signal processing, machine learning, and AI-driven technologies.
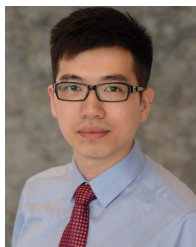
Baiping Xiong received the B.Eng. degree in information engineering from Southeast University, Nanjing, China, in 2019. He is currently pursuing the Ph.D. degree with the National Mobile Communications Research Laboratory, Southeast University, Nanjing.

Zaichen Zhang (Senior Member, IEEE) was born in Nanjing, China, in 1975. He received the B.S. and M.S. degrees in electrical and information engineering from Southeast University, Nanjing, in 1996 and 1999, respectively, and the Ph.D. degree in electrical and electronic engineering from The University of Hong Kong, Hong Kong, in 2002. From 2002 to 2004, he was a Post-Doctoral Fellow with the National Mobile Communications Research Laboratory, Southeast University. In 2004, he joined the School of Information Science and Engineering, Southeast University, where he is currently a Professor. He has published more than 200 articles and issued 50 patents. His current research interests include 6G mobile communication systems, optical wireless communications, and quantum information processing.

Hongming Zhang (Member, IEEE) received the B.Eng. degree (Hons.) in telecommunications from the Nanjing University of Aeronautics and Astronautics (NUAA) and the City University of London, in 2011, and the M.Sc. and Ph.D. degrees in wireless communications from the University of Southampton in 2012 and 2017, respectively. From 2017 to 2018, he was with the Department of Electrical Engineering, Columbia University, New York, NY, USA. He is currently an Assistant Professor with the School of Information and Communication Engineering, Beijing University of Posts and Telecommunications, Beijing, China. His research interests include wireless communications, heterogeneous network performance analysis and optimization, and machine learning.

Jian Dang (Senior Member, IEEE) received the B.S. degree in information engineering and the Ph.D. degree in information and communications engineering from Southeast University, Nanjing, China, in July 2007 and September 2013, respectively. From September 2010 to March 2012, he was a Visiting Scholar with the Department of Electrical and Computer Engineering, University of Florida, USA. Since September 2013, he has been with the National Mobile Communications Research Laboratory, Southeast University, where he is currently an Associate Professor. His research interests include signal processing in wireless communications and optical mobile communications.

Jiangfan Zhang (Member, IEEE) received the B.Eng. degree in communication engineering from the Huazhong University of Science and Technology, Wuhan, China, in 2008, the M.Eng. degree in information and communication engineering from Zhejiang University, Hangzhou, China, 2011, and the Ph.D. degree in electrical engineering from Lehigh University, Bethlehem, PA, USA, in 2016. From 2016 to 2018, he was a Post-Doctoral Research Scientist with the Department of Electrical Engineering, Columbia University, New York, NY, USA. Since 2018, he has been with the Department of Electrical and Computer Engineering, Missouri University of Science and Technology, Rolla, MO, USA, where he is currently an Assistant Professor. His research interests include signal processing, machine learning, and their applications to cybersecurity, cyber-physical asystems, the Internet of Things, smart grid, and sonar processing.

Dr. Zhang was a recipient of the Dean's Doctoral Student Assistantship, Gotshall Fellowship, and a P. C. Rossin Doctoral Fellow at Lehigh University.

Liang Wu (Member, IEEE) received the B.S., M.S., and Ph.D. degrees from the School of Information Science and Engineering, Southeast University, Nanjing, China, in 2007, 2010, and 2013, respectively. From September 2011 to March 2013, he was a Visiting Ph.D. Student with the School of Electrical Engineering and Computer Science, Oregon State University. In September 2013, he joined the National Mobile Communications Research Laboratory, Southeast University, where he has been an Associate Professor since April 2018. His research interests include optical wireless communications, multiple input and multiple output technology, interference alignment, and wireless indoor localization.